Regulation of defective mitochondrial DNA accumulation and transmission in *C. elegans* by the programmed cell death and aging pathways

Sagen E. Flowers[1], Rushali Kothari[1], Yamila N. Torres Cleuren[1,2], Melissa R. Alcorn[1], Chee Kiang Ewe[1], Geneva Alok[1], Pradeep M. Joshi[1], Joel H. Rothman[1]

Affiliations:

1. Department of MCD Biology and Neuroscience Research Institute, University of California Santa Barbara, CA, USA
2. Computational Biology Unit, Institute for Informatics, University of Bergen, Norway

To whom correspondence should be addressed: rothman@lifesci.ucsb.edu

Keywords: heteroplasmy, uaDf5, purifying selection, programmed cell death, aging, insulin signaling

ORCiD:

SEF - 0000-0002-7818-2188

YNTC- 0000-0003-2218-7243

MRA- 0000-0001-6284-3255

CKE - 0000-0003-1973-1308

GA- 0000-0001-6257-2344

PMJ- 0000-0002-4220-0559

JHR - 0000-0002-6844-1377

Abstract

The heteroplasmic state of eukaryotic cells allows for cryptic accumulation of defective mitochondrial genomes (mtDNA). "Purifying selection" mechanisms operate to remove such dysfunctional mtDNAs. We found that activators of programmed cell death (PCD), including the CED-3 and CSP-1 caspases, the BH3-only protein CED-13, and PCD corpse engulfment factors, are required in *C. elegans* to attenuate germline abundance of a 3.1 kb mtDNA deletion mutation, *uaDf5*, which is normally stably maintained in heteroplasmy with wildtype mtDNA. In contrast, removal of CED-4/Apaf1 or a mutation in the CED-4-interacting prodomain of CED-3, do not increase accumulation of the defective mtDNA, suggesting induction of a non-canonical germline PCD mechanism or non-apoptotic action of the CED-13/caspase axis. We also found that the abundance of germline mtDNA^{uaDf5} reproducibly increases with age of the mothers. This effect is transmitted to the offspring of mothers, with only partial intergenerational removal of the defective mtDNA. In mutants with elevated mtDNA^{uaDf5} levels, this removal is enhanced in older mothers, suggesting an age-dependent mechanism of mtDNA quality control. Indeed, we found that both steady-state and age-dependent accumulation rates of *uaDf5* are markedly decreased in long-lived, and increased in short-lived, mutants. These findings reveal that regulators of both PCD and the aging program are required for germline mtDNA quality control and its intergenerational transmission.

41 **Introduction**

42 Mitochondrial diseases are a group of conditions that affect mitochondrial functions in
43 up to 1 in 4,300 people [1–3]. Generally, these diseases present as dysfunction in the tissues or
44 organs with the most intensive energy demands, most commonly in muscle and the nervous
45 system [4]. Many of these diseases are attributable to mutations in the mitochondrial DNA
46 (mtDNA) or nuclear DNA (nDNA), and include those disorders with defects in mitochondrial
47 function, dynamics, or quality control, or in which there is miscommunication between the
48 mitochondria and the endoplasmic reticulum (ER) [3,5]. The progressive advancement of the
49 diseased state resulting from age-dependent accumulation of mutant mtDNA is a common trait
50 among mitochondrial diseases [6–8]. While the severity of the disease varies with the nature of
51 the mutation, the most severe phenotypes result in childhood death, as in Leigh syndrome and
52 MELAS [5,9]. As there are currently no pharmacological treatments for mitochondrial diseases, it
53 is of great importance to uncover the cellular processes that underlie the regulation of mtDNA
54 quality control.

55 mtDNAs show high mutation rates [10–12] and hence it is critical that cells possess
56 mechanisms to remove detrimental mtDNA alleles, a process called purifying selection [13,14].
57 Defects in this process can result in mitochondrial diseases, allowing harmful mtDNA mutations
58 to persist through the maternal germline and subsequent generations. Processes that regulate
59 mtDNA quality control include mitochondrial fission/fusion dynamics and mitophagy [8,15–20],
60 and the mitochondrial unfolded protein response (UPR^{MT}; [21–27]. Further, it has also been
61 found that the insulin/IGF-1 signaling pathway (IIS; [28,29]) ameliorates the fitness defects of
62 mutant mtDNA.

63 One potential cellular process that could be used to eliminate defective mtDNAs is the
64 culling of cells bearing mtDNA mutations by programmed cell death (PCD). The mechanisms of
65 both developmentally controlled and genotoxicity-induced PCD have been shown to be well-
66 conserved across metazoans [30], and much of the machinery that choreographs this process is
67 directed by mitochondria [31–33]. Mitochondrial-dependent processes participating in PCD
68 include permeabilization of the inner mitochondrial membrane and release of mitochondrial
69 factors that mediate transduction of intermediary events in the cell suicide program [31–33].
70 Both mitochondrial function and PCD are linked to the process of organismal aging [34]. mtDNA
71 mutations accumulate in tissues as organisms age, and it has been suggested that this
72 accumulation is a major contributor to aging [35–37].

73 The nematode *C. elegans* provides an attractive model for exploring the potential role of
74 PCD in mtDNA purifying selection. The well-described, conserved PCD regulatory pathway in *C.*
75 *elegans* functions not only to eliminate 131 somatic cells during development through a rigidly
76 stereotyped program [38], but is also activated apparently stochastically during germline
77 development, resulting in the death of >95% of nuclei that would otherwise be destined to
78 become oocytes in the mature hermaphrodite [30,39–41]. In addition to this "physiological" PCD,
79 germline nuclei that have experienced genotoxic stress are eliminated through p53-dependent
80 apoptosis, as is also the case in somatic mammalian cells [42,43]. Thus, germline PCD allows for
81 selective removal of nuclei with damaged genomes, thereby preventing intergenerational
82 transmission of defective nuclear DNA. Given the prominent role played by mitochondria in the
83 PCD process, it is conceivable that mitochondrial dysfunction could trigger PCD in the germline

84 and, as such, might similarly provide a quality control mechanism for eliminating aberrant
85 mtDNA, as seen for the nuclear genome.

86 We report here that germline mtDNA quality control in *C. elegans* is influenced by
87 regulators of both PCD and the aging program. We find that pro-apoptotic regulators of germline
88 PCD, notably the caspases CED-3 and CSP-1, the BH3-only domain protein CED-13, and regulators
89 of cell corpse engulfment, reduce abundance of an mtDNA deletion and that abrogation of their
90 functions results in elevated levels of the defective mtDNA. Notably, however, loss of the CED-3
91 activator CED-4/Apaf1 [44,45] does not result in elevated levels of defective mtDNA. These
92 findings raise the possibilities that either the caspases and the other pro-apoptotic factors
93 function in mtDNA purifying selection by a non-canonical CED-4-independent cell death program,
94 or that these pro-apoptotic regulators function in mtDNA purifying selection through a PCD-
95 independent mechanism. We also report that defective mtDNA accumulates in the germline of
96 animals with age and that although the abundance of the defective mtDNA is reduced in
97 offspring, progeny of older mothers inherit higher levels of the mutant mtDNA than those from
98 young mothers. Intergenerational removal of the defective mtDNA appears to be enhanced in
99 older animals with defective mtDNA quality control. Further, we found that lifespan-extending
100 mutations in both the IIS pathway and the non-IIS-dependent lifespan-regulator CLK-1/MCLK1
101 decrease accumulation of defective mtDNA, and that short-lived mutants show elevated
102 accumulation, implicating molecular regulators of the aging process in mtDNA purifying
103 selection. Our findings reveal that the PCD machinery and the aging program contribute to the
104 removal of mtDNA mutations during germline development and their intergenerational
105 transmission.

106

107 **Results**

108 **The stably maintained mtDNA deletion mutant *uaDf5* contains multiple linked mutations**

109 **resulting in aberrant proteins and shows deleterious effects on growth**

110 To test the role of potential regulatory factors in mtDNA purifying selection, we took

111 advantage of *uaDf5*, a 3.1 kb mtDNA deletion mutation that removes part or all of four protein-

112 coding genes and seven tRNAs (Fig. 1A) [46]. Given the presumably deleterious nature of this

113 defective mtDNA, it was of interest to understand how it is stably transmitted despite active

114 purifying selection processes. While its maintenance at high levels is attributable in part to

115 stabilization by the mitochondrial UPR [25], *uaDf5* persists, albeit at lower levels, in animals

116 lacking this activity. One possible explanation for this phenomenon is that the mutant mtDNA

117 might be maintained in heteroplasmy with an otherwise intact mtDNA carrying a complementing

118 mutation. We sought to test this possibility through deep sequencing of mtDNA isolated from

119 the *uaDf5*-bearing strain. Comprehensive sequence analysis revealed that, in addition to the

120 large deletion, the strain indeed carries a second mtDNA mutation, *w47* (Fig. 1A, Suppl. Fig. 1A,

121 B, C). *w47* is a single base pair insertion in the *nduo-4* gene that causes a frameshift, predicted to

122 result in a truncated NADH dehydrogenase 4 (ND4) protein lacking 321 residues (Suppl. Fig. 1D).

123 ND4 is an essential transmembrane subunit within complex I of the mitochondrial respiratory

124 chain (MRC), which drives NADH-oxidation-dependent transport of protons across the inner

125 mitochondrial membrane [47–49]. While this raised the possibility of two complementing mtDNA

126 genomes, we found that the *w47* mutation is present at the same abundance as the *uaDf5*

127 deletion mutation (~75% of total mtDNA, Suppl. Fig. 1B) rather than that of the wild-type mtDNA,

128 strongly suggesting that it resides on the same mtDNA genome. As this second mutation cannot

129 explain stabilization of the defective mtDNA by *trans*-complementation of two deleterious
130 mutations, other mechanisms appear to promote the stable inheritance of *uaDf5*.

131 In addition to the aberrant protein encoded by the *w47* frameshift mutation in *nduo-4*, a
132 second abnormal protein is encoded by the *uaDf5* genome: one end of the deletion results in a
133 fusion protein comprised of the first 185 amino acids of NADH dehydrogenase 1 (ND1, a homolog
134 of the core MT-ND1 transmembrane subunit of complex I of the MRC [47,49,50]), and the last 81
135 amino acids of mitochondrial-encoded cytochrome b (CTB-1/CYTB, a transmembrane subunit of
136 complex III of the MRC [47,49,51]) (Suppl. Fig. 1E). It is conceivable that accumulation of these
137 two abnormal proteins -- the truncated ND4 and the ND1-CYTB fusion protein resulting from *w47*
138 and *uaDf5*, respectively – activate the UPR^{MT}, which has been shown to result in clearance of
139 $mtDNA^{uaDf5}$, dependent on the ATFS-1 transcription factor [25,27].

140 Animals harboring $mtDNA^{uaDf5}$ are viable and fertile, presumably because they contain
141 intact wildtype mtDNA [46]. However, we found that *uaDf5*-bearing animals displayed a
142 significant reduction in brood size (WT 304 ± 4.8; *uaDf5* 201 ± 8.6 embryos laid, $p < 0.001$) (Fig.
143 1B) and a significant increase in embryonic lethality (WT 1.4 ± 0.2%; *uaDf5* 4.2 ± 0.7%, $p < 0.001$)
144 (Fig. 1C). Additionally, *uaDf5* animals are slow-growing, evident in both the number of hours to
145 reach gravidity (WT 63 ± 0.8; *uaDf5* 76 ± 1.4 hours at 20°C, $p < 0.001$) (Fig. 1D) and the stage of
146 development reached after 60 hours of feeding (WT: adult; *uaDf5:* mid-L4) (Fig. 1E). In contrast,
147 however, we were surprised to find that lifespan was not substantially affected (WT 14 ± 0.4;
148 *uaDf5* 15 ± 0.5 days) (Fig. 1F, Suppl. Fig. 2). Given the significant decline in the majority of fitness
149 parameters tested, we conclude that *uaDf5* is a useful tool for studying mitochondrial disease
150 and mechanisms underlying mtDNA quality control.

151 **PCD regulators promote removal of mtDNA^{uaDf5}**

152 During germline development in *C. elegans*, as many as 95% of nuclei destined to become
153 potential oocytes are eliminated by PCD [39–41,52]. While this process has been proposed to be
154 stochastically determined [39,52], it has also been suggested that it may function to selectively
155 remove all but the most "fit" germline cells. As such, PCD could perform a role in purifying
156 selection in the germline, wherein potential oocytes that undergo PCD are associated with higher
157 levels of defective mtDNA. To test this hypothesis, we introduced *uaDf5* into various PCD mutants
158 and quantified abundance of the defective mtDNA by digital-droplet PCR (ddPCR; see
159 Supplementary Table 1 for list of mutants tested). In a wildtype genetic background, we found
160 that the steady-state fractional abundance of *uaDf5* in populations of 200 day 1 adults (first day
161 of adulthood) is highly reproducible across four separate trials, demonstrating the reliability and
162 robustness of the assay. Our analyses confirmed that mtDNA^{uaDf5} constitutes the major molar
163 fraction of mtDNA in the *uaDf5*-bearing strain by a nearly 3:1 ratio (Suppl. Fig. 3).

164 CED-3 in *C. elegans* is the major executioner caspase in the canonical PCD pathway
165 [38,52,53] and is required for virtually all PCD both in the germline and the soma (Suppl. Fig. 5).
166 We found that two *ced-3* mutations that strongly block PCD [54] showed a significant increase in
167 the ratio of defective to normal mtDNA from a molar ratio of 2.9:1 for *ced-3(+)* to 3.5:1 for *ced-*
168 *3(n717)* and 4.6:1 for *ced-3(n1286)* (Fig. 2A). This effect appears to be exclusively attributable to
169 an increase in mtDNA^{uaDf5} in the PCD-deficient strains, as the abundance of mtDNA^{WT} is not
170 significantly different between the strains. These *ced-3(-)* mutations both localize to the p15
171 domain of the protease portion of CED-3 (Suppl. Fig. 4), consistent with abolition of caspase
172 activity. These findings implicate the CED-3 caspase and its p15 domain in mtDNA quality control.

173 We found that one other mutation located in the p15 domain showed only a very slight increase
174 that was not statistically significant (*n2454:* 2.9:1, Fig. 2B). While it is unclear why this allele
175 showed a weaker effect it is noteworthy that, unlike the other two mutations, which result in a
176 dramatic alteration of the protein, this mutation is predicted to result in a relatively modest (ala
177 → thr) single amino acid substitution.

178 A second caspase in *C. elegans*, CSP-1, also functions, albeit less prominently, in PCD.
179 While loss of CSP-1 alone does not result in a strong reduction in PCD, it synergizes with loss of
180 CED-3 both in PCD and in other caspase-dependent processes (Suppl. Fig. 5) [55–57]. We found
181 that removing CSP-1 in the *csp-1(tm917)* knockout mutant results in a significant increase in
182 mtDNA^{uaDf5} abundance to a molar ratio of 3.9:1 (Fig. 2A). Further, we found that this mutation
183 enhances the effect of the *ced-3(n717)* mutation, increasing the mtDNA^{uaDf5}:mtDNA^{WT} molar
184 ratio from 3.5:1 to 4.7:1 (Fig. 2A). Together these findings demonstrate that caspase activity, and
185 possible PCD-mediated clearance, are crucial for mtDNA quality control and function in purifying
186 selection of defective mtDNA.

187 We sought to further investigate a potential role for PCD in mtDNA purifying selection by
188 evaluating the requirement for the pro-apoptotic factor CED-13, a BH3-only domain protein that
189 acts specifically in the germline to activate PCD [38,58,59]. Consistent with a requirement for PCD
190 in purifying selection, we found that two *ced-13* alleles result in a very substantial increase in the
191 mtDNA^{uaDf5}:mtDNA^{WT} molar ratio (*sv32*: 4.2:1 and *tm536*: 5.1:1) (Fig. 2A), supporting the notion
192 that CED-13 promotes removal of defective mtDNA in the germline. CED-13 functions in PCD by
193 antagonizing the function of mitochondrially localized CED-9/Bcl-2 [58,59], which normally
194 sequesters the apoptosome factor CED-4/APAF1 at mitochondria, thereby preventing it from

195 triggering autocatalytic conversion of the executioner caspase zymogen proCED-3 to its pro-
196 apoptotic protease structure (Suppl. Fig. 5) [60]. An equivalent action is carried out in the soma
197 by the BH3-only protein EGL-1 [60]. *n1950*, a gain-of-function allele of *ced-9* that blocks the
198 interaction of EGL-1 with CED-9 at the mitochondria, results in elimination of PCD in the soma
199 but not the germline [39,52,60,61]. Consistent with the lack of effect of *ced-9(n1950gf)* on
200 germline PCD, we found that the mtDNA^{uaDf5}:mtDNA^{WT} molar ratio was not increased in *ced-*
201 *9(n1950gf)* mutants (2.2:1) (Fig. 2B). Thus, CED-3, CSP-1, and CED-13 are required both for
202 germline PCD and for removal of mtDNA^{uaDf5}.

203 Cells that undergo PCD are cleared by the surrounding cells in the process of engulfment
204 and degradation, which is implemented through a set of redundant pathways that converge on
205 the CED-10 GTPase [62–65] (Suppl. Fig. 5). Although this engulfment process is necessary
206 primarily for removal of the resultant corpses, it also appears to play an active role in cell killing:
207 inhibition of the engulfment pathway diminishes occurrence of PCD, likely through a complex
208 feedback mechanism [66,67]. Further supporting a role for PCD in purifying selection, we found
209 that single or double mutations of several genes that promote engulfment of cell corpses result
210 in elevated mtDNA^{uaDf5}:mtDNA^{WT} molar ratios, ranging from 3.5:1 to 5.2:1 (4.1:1 for *ced-*
211 *1(e1735)*, 4.5:1 for *ced-2(e1752)*, 5.2:1 for the *ced-1(e1735); ced-2(e1752)* double mutant, 3.6:1
212 for *ced-10(n1993)*, and 4.8:1 for *ced-10(n3246)*; Fig. 2A).

213 We tested whether *generally* increased germline PCD alters mtDNA^{uaDf5} abundance by
214 examining the effect of removing the caspase-related factor, CSP-2, which has been shown to
215 play an anti-apoptotic role through inhibition of CED-3 autoactivation in the germline (Suppl. Fig.
216 5) [68]. We found that a loss-of-function mutation in *csp-2*, which elevates germline PCD, did not

217 alter the mtDNA^{uaDf5}:mtDNA^{WT} molar ratio (2.9:1 for the *csp-2(tm3077)* knockout mutation) (Fig.
218 2B). This observation does not conflict with a requirement for PCD in purifying selection: a
219 general increase in PCD in the germline of *csp-2(-)* animals would not be expected *per se* to alter
220 the mechanism that *discriminates* defective from normal mtDNAs and therefore the relative
221 abundance of the two forms. Rather, our findings suggest that the mechanisms that recognizes
222 and disposes of the defective mtDNA specifically requires PCD components acting in a selective,
223 rather than general process (i.e., in those cells with the highest burden of the defective mtDNA).
224

225 **Evidence for non-canonical action of PCD regulators in mtDNA purifying selection**

226 The foregoing results implicate a role for the pro-apoptotic CED-3 and CSP-1 caspases,
227 CED-13, and the CED-1, 2, and -10 cell corpse engulfment factors in mtDNA purifying selection.
228 However, several observations suggest that elimination of normal, physiological germline PCD
229 *per se* is insufficient to increase accumulation of defective mtDNA, or that these factors promote
230 purifying selection through a PCD-independent pathway. Specifically, we observed that the
231 occurrence of PCD does not perfectly correlate with their effects on accumulation of mtDNA^{uaDf5}
232 in particular mutants.

233 First, we found that the *ced-3*(*n718)* allele lowers, rather than elevates, the abundance of
234 mtDNA^{uaDf5} (mtDNA^{uaDf5}:mtDNA^{WT} molar ratio of 1.8:1, Fig. 2C). This effect is likely to be
235 attributable to the nature of the *n718* mutation. Those *ced-3* mutations that result in increased
236 mtDNA^{uaDf5} levels (Fig. 2A) both alter the p15 domain, which is essential to the active caspase
237 function. In contrast, the *n718* mutation changes a residue in the caspase activation and
238 recruitment domain (CARD), located within the prodomain of the CED-3 zymogen, which is

239 removed upon caspase activation and affects its activation by CED-4 (Suppl. Fig. 4) [44,54]. While
240 *ced-3*(*n718)* strongly compromises PCD, this mutation might not alter CED-3 caspase function in
241 a way that interferes with its role in mtDNA purifying selection.

242 Our surprising finding that while CED-3 activity is required for mtDNA purifying selection,
243 a CED-3 mutation that compromises its activation by CED-4 did not elevate mtDNA^{uaDf5} levels
244 prompted us to investigate the requirement of CED-4 in mitochondrial purifying selection.
245 Consistent with the effect of the *ced-3*(*n718)* mutation, we found that eliminating the function
246 of the pro-apoptotic regulator CED-4, the *C. elegans* orthologue of mammalian Apaf1 and the
247 upstream activator of CED-3 in the canonical PCD pathway [60,69], did not result in a marked
248 increase in the relative abundance of mtDNA^{uaDf5}. That is, while the mtDNA^{uaDf5}:mtDNA^{WT} molar
249 ratio increased to 3.1:1 in the *ced-4(n1894)* mutant, the effect was not statistically significant.
250 Moreover, the canonical allele *ced-4(n1162)* allele similarly showed no elevation in mtDNA^{uaDf5}
251 (molar ratio = 2.6:1; Fig. 2B). These results suggest that CED-3 caspase functions in mitochondrial
252 purifying selection independently of the caspase-activating factor CED-4.

253

254 **Evidence that decreased fitness, but not lifespan, is attributable to mtDNA^{uaDf5}-induced PCD**

255 Taken together, our results implicate many PCD regulatory factors, and potentially PCD, in
256 the selective clearance of defective germline mtDNAs. Our additional observations suggest that
257 defective mtDNAs may, in fact, *trigger* elevated germline PCD, resulting in the production of
258 fewer mature gametes and progeny. Specifically, we found that the significant decrease in brood
259 size that we observed in *uaDf5*-bearing animals with a wildtype nuclear background is partially
260 suppressed by both *ced-3(-)* and *ced-13(-)* mutations, which prevent PCD (Fig. 2D, Suppl. Fig. 6A),

261 suggesting that elimination of PCD might rescue cells that would otherwise be provoked to die
262 as a result of accumulation of defective mtDNA. Our findings further underscore the observation
263 that accumulation of defective mtDNA in those animals that do survive does not affect longevity,
264 as we found that lifespan is unaltered in these PCD mutants even when the levels of mtDNA^{uaDf5}
265 are nearly doubled (Suppl. Fig. 6B, C).
266

267 **Age-dependent accumulation of mtDNA^{uaDf5} in the germline**

268 Our findings that PCD regulators are required to reduce mtDNA^{uaDf5} abundance, the
269 central role that mitochondria play in PCD [31–33,70], the observed decline of mitochondrial
270 health during the aging process [7,35–37,71–75], and the relationship between excessive PCD
271 and the aging phenotype [34] led us to examine the dynamics of mtDNA^{uaDf5} accumulation as
272 worms age. We measured the fractional abundance of *uaDf5* in adults at progressively increased
273 ages spanning day 1, defined as the first day of egg-laying, through day 10. Day 1 through day 4
274 of adulthood encompasses the time during which nearly all self-progeny are produced. After day
275 4, hermaphrodite sperm become depleted and the animals transition into a post-gravid,
276 progressively aging state [76–78]. By day 10, animals exhibit indications of advanced age. Analysis
277 of the abundance of mtDNA^{uaDf5} revealed a progressive increase throughout gravidity and post-
278 reproductive aging, with the mtDNA^{uaDf5}:mtDNA^{WT} molar ratio increasing from 2.9:1 to 5.5:1 (Fig.
279 3A, Suppl. Fig. 7A). This age-related accumulation of *uaDf5* in adult worms is reminiscent of the
280 accumulation of mtDNA mutations seen in aging mammals [35,73,79] and suggests that *uaDf5* in
281 *C. elegans* may be a useful tool for studying the role that mtDNA mutations play in aging.

282 Given that gametes are depleted with age, it is conceivable that the age-dependent
283 increase in mtDNA^{uaDf5} is attributable to accumulation in somatic mitochondria. To assess
284 whether the observed age-related accumulation of mtDNA^{uaDf5} occurs predominantly in the
285 maternal germline or in somatic cells, we analyzed animals defective in germline development
286 by taking advantage of the *glp-4(bn2)* mutant, which produces only a small number (~12) of
287 germline cells compared to that in wildtype animals (~1,500), with no known effect on somatic
288 gonad development [80]. In contrast to the increased mtDNA^{uaDf5} abundance with age seen at
289 permissive temperature (mtDNA^{uaDf5}:mtDNA^{WT} of 1.8:1 at day 1, rising to 2.6:1 at day 4, for an
290 overall increase by 48%), we found that *glp-4(bn2)* animals at the non-permissive temperature
291 showed a slight decrease in the defective mtDNA from day 1 to day 4 of adulthood (2.2:1 at day
292 1, dropping to 2:1 at day 4, for an overall decrease of 6.3%) (Fig. 3B). These results strongly
293 suggest that the observed age-dependent increase in mtDNA^{uaDf5} abundance occurs exclusively
294 in the germline. We found that mtDNA^{uaDf5} does eventually appear to accumulate in somatic cells
295 with age, as day 10 adults grown at the restrictive temperature showed a marked increase in the
296 mtDNA^{uaDf5}:mtDNA^{WT} molar ratio compared to day 1 adults even in the absence of a germline
297 (day 10 *glp-4(bn2)* molar ratio of 3.4:1, a 57% increase from day 1 levels) (Fig. 3B). We conclude
298 that the marked increase in mtDNA^{uaDf5} with age during the period of fecundity occurs primarily
299 in the germline and that the defective mtDNA accumulates in both germline and somatic tissue
300 during post-reproductive life.
301
302 **Age-dependent increase in mtDNA^{uaDf5} burden is transmitted to progeny**

303 As the mtDNA is inherited strictly through the maternal germline, we posited that the
304 age-dependent increase in the fractional abundance of germline mtDNA^{uaDf5} might be
305 transmitted to progeny animals. To test this hypothesis, we measured the molar ratio of
306 mtDNA^{uaDf5} in 200-worm populations of L1 larvae derived from day 1 – day 4 adults (Fig. 3C,
307 Suppl. Fig. 7B). This analysis led to two key observations: 1) the abundance of mtDNA^{uaDf5} is
308 reduced during transmission between mother and offspring (average decrease ranging from 6%
309 to 13%), presumably as a result of purifying selection, and 2) the abundance of the defective
310 mtDNA in the offspring correlates with the age of the mothers: the progeny of older mothers
311 contain a markedly higher mtDNA^{uaDf5}:mtDNA^{WT} molar ratio (4.2:1) than that of younger mothers
312 (2.6:1) (Fig. 3C, D). A similar trend was observed for mother-to-offspring transmission in five
313 mutant strains with altered levels of mtDNA^{uaDf5} (see below): in all cases, progeny contain lower
314 abundance of mtDNA^{uaDf5} than their mothers, and progeny of younger adults inherit a lower load
315 of mtDNA^{uaDf5} than progeny of older adults (Fig. 3C). These results reveal that mtDNA quality
316 control occurs between primordial germ cell proliferation in the female germline and L1 hatching,
317 i.e., during oocyte maturation, embryogenesis, or both.
318

319 **The lifespan-determining IIS pathway regulates accumulation of mtDNA^{uaDf5}**

320 We sought to determine whether the age-dependent accumulation of defective mtDNA
321 is controlled by known molecular mechanisms that drive the aging program in *C. elegans*. The
322 most prominent of these regulatory systems is the highly conserved insulin/IGF-1 (insulin-like
323 growth factor-1) pathway (IIS), which performs a pivotal regulatory function in aging and
324 longevity [28,82,83] (Suppl. Fig. 8). Abrogation of the IIS signaling pathways, for example, as a

325 result of mutations in the gene encoding the IIS receptor (DAF-2, in *C. elegans*), results in marked
326 slowing of the aging program and extension of lifespan in worms, flies, and mice [84–87]. The IIS
327 pathway also functions in a broad set of other processes including, in *C. elegans*, activation of
328 two stages of developmental arrest, or diapause, at the L1 larval stage and in formation of the
329 dispersal form, the dauer larva, as well as in the control of germline proliferation, stress
330 resistance, fat metabolism, and neuronal/behavioral programs [28]. It was also reported that
331 inhibition of the IIS pathway rescues various fitness parameters in a mtDNA mutator strain which
332 contains a faulty mtDNA polymerase [29], consistent with a possible role in mtDNA quality
333 control.

334 We found that two mutant alleles of *daf-2*, which reduce rates of aging and increase
335 lifespan, result in dramatically decreased mtDNA^{uaDf5}:mtDNA^{WT} molar ratios from 2.8:1 to as low
336 as 0.3:1 (0.3:1 for *daf-2(e1391*); 0.8:1 for *daf-2(e1370)*; Fig. 4A; see Suppl. Table 2 for a list of
337 lifespan mutants used in the analyses). Thus, the lifespan-extending effects of *daf-2* mutations
338 are strongly correlated with diminished abundance of defective mtDNA, to the extent that it
339 becomes the minor species of mtDNA.

340 The DAF-2 receptor acts by antagonizing the DAF-16/FoxO transcription factor, the major
341 effector of IIS downstream, in response to insulin-like ligands. Thus, removal of *daf-16* function
342 reverses the lifespan-extending effects of *daf-2(-)* mutants. We tested whether the DAF-2 → DAF-
343 16 pathway similarly functions in mtDNA purifying selection. We found that eliminating DAF-16
344 in two *daf-16* mutants results in slightly increased, albeit not statistically significant,
345 mtDNA^{uaDf5}:mtDNA^{WT} molar ratios (3.3:1 for *daf-16(mu86)*; 3.5:1 for *daf-16(mgDf50)*) (Fig. 4B).
346 Further, we found that removal of DAF-16 in the *daf-16(mu86)* mutant suppressed the decreased

347 mtDNA^{uaDf5}:mtDNA^{WT} molar ratios observed in two *daf-2* mutants, from 0.3:1 for *daf-2(e1391)* to
348 1:1 for *daf-16(mu86); daf-2(e1391)* and from 0.6:1 for *daf-2(e1370)* to 1.8:1 for *daf-16(mu86);*
349 *daf-2(e1370)*, consistent with observations reported in a recent study [88]. While the *daf-2(-)*
350 effect on mtDNA^{uaDf5} levels is largely dependent on DAF-16, neither double mutant restored
351 mtDNA^{uaDf5} levels to those seen in animals with a fully intact IIS pathway, suggesting that other
352 DAF-2 targets might participate in removal of defective mtDNA (Fig. 4C). We found, conversely,
353 that two mutations that reduce lifespan by eliminating the function of AAK-2 (AMP activated
354 kinase-2), a conserved factor acting in the IIS pathway [28,89], result in elevated
355 mtDNA^{uaDf5}:mtDNA^{WT} molar ratios as high as 4.4:1 compared to 2.8:1 in wildtype animals (3.8:1
356 for *aak-2(ok524)* and 4.4:1 for *aak-2(gt33)*) (Fig. 4B). These findings demonstrate that alterations
357 in the IIS pathway coordinately affect both lifespan and accumulation of defective mtDNA and
358 that the DAF-2/DAF-16/AAK-2 axis acts similarly in both processes.
359
360 **Synergistic effect of multiple aging pathways on mtDNA^{uaDf5} accumulation**
361 In addition to IIS, other molecular regulatory pathways independently contribute to the
362 rate of aging. These include CLK-1, a mitochondrial hydroxylase that functions in the pathway for
363 ubiquinone synthesis [90,91]. *clk-1* mutants with a wildtype mitochondrial genome have been
364 shown to contain levels of mtDNA that are elevated by 30%, perhaps as the result of a
365 compensatory process that increases demand on mitochondrial abundance, or the action of CLK-
366 1 as a regulator of mtDNA abundance in response to energy availability within the cell [92]. As
367 with long-lived *daf-2* mutants, we found that long-lived *clk-1(qm30)* mutants showed a greatly
368 diminished mtDNA^{uaDf5}:mtDNA^{WT} molar ratio of 0.3:1 (Fig. 4A), comparable to that in *daf-2*

369 mutants; again, mtDNA^{uaDf5} is the minor species in these animals. As the IIS pathway and CLK-1
370 appear to act separately in controlling lifespan, we postulated that elimination of both
371 mechanisms might further reduce levels of the defective mtDNA. Indeed, we found that
372 mtDNA^{uaDf5} was completely eliminated in *daf-2(e1391) clk-1(qm30)* double mutants, revealing a
373 strongly synergistic effect between the two age-determining systems (Fig. 4A). Thus, distinct
374 regulatory pathways for longevity modulate the abundance of mtDNA^{uaDf5} by apparently different
375 mechanisms and elimination of the two pathways abrogates its maintenance.
376

377 **Age-dependent accumulation rate of mtDNA^{uaDf5} strongly correlates with genetically altered**
378 **rates of aging**

379 Our findings that the steady-state abundance of mtDNA^{uaDf5} increases with maternal age
380 and that mutants with increased lifespan show lower levels of the defective mtDNA raised the
381 possibility that purifying selection is subject to the same control as aging clocks. To assess this
382 potential connection, we analyzed the time-dependent rates of mtDNA^{uaDf5} accumulation in
383 animals with genetic backgrounds that alter the aging clock. Analysis of 21 different genetic
384 backgrounds over the first ten days of adulthood revealed that the age-dependent progressive
385 accumulation of mtDNA^{uaDf5} is a consistent phenomenon (Fig. 4D). Comparison of long-lived
386 mutants and wildtype using a linear regression model revealed a striking positive correlation
387 between aging rate and age-dependent rate of accumulation of mtDNA^{uaDf5}: all long-lived
388 mutants in either the IIS pathway or *clk-1* accumulate mtDNA^{uaDf5} at a substantially slower rate
389 as they age than do wildtype animals (Fig. 4E, Suppl. Fig. 9A, B). Conversely, we analyzed six short-
390 lived IIS pathway mutant combinations and found that the *aak-2(ok524)* and *daf-16(mu86)* single

391 mutants and *daf-16(-);daf-2(-)* double mutants all showed increased rates of mtDNA^{uaDf5}
392 accumulation (Fig. 4E, Suppl. Fig. 9C, D). These observations suggest that in both slower-aging
393 and faster-aging strains, the rate of accumulation of deleterious mtDNA is a predictor of aging
394 rate. In the two exceptional cases, the *aak-2(gt33)* and *daf-16(mgDf50)* single mutants, we did
395 not observe an increased accumulation rate compared to wildtype; however, the mtDNA^{uaDf5}
396 levels are consistently higher than in these two mutants than in wildtype at all stages (Fig. 4E,
397 Suppl. Fig. 9D) and thus diminished removal of mtDNA^{uaDf5} overall correlates with decreased
398 lifespan in these mutants as well. The greater mtDNA^{uaDf5} accumulation rates seen in the short-
399 lived animals is not attributable to the higher steady-state levels *per se*, as the rates of
400 accumulation of defective mtDNA observed in the PCD mutants with higher mtDNA^{uaDf5} levels
401 show no correlation with the steady-state levels (Suppl. Fig. 9 E-H); rather these increased rates
402 appear specifically to be a property of the shortened lifespan mutants.

403 Consistent with a relationship between aging rates and accumulation of defective mtDNA,
404 we found that brood size is decreased and embryonic lethality is increased in short-lived *daf-16(-*
405 *)* mutants compared to those in a wildtype nuclear background, while *uaDf5* does not impact
406 either fitness parameter in the long-lived *clk-1* mutant (Suppl. Fig. 10). These results are
407 consistent with the possibility that longevity pathways modulate fitness in part by regulating
408 mitochondrial homeostasis.

409

410 **Evidence for late adulthood-specific mechanisms for removal of mtDNA^{uaDf5}**

411 We obtained evidence that defective mtDNA is more effectively removed in offspring of
412 aging adults that carry an unusually high burden of mtDNA^{uaDf5}. The offspring of day 4 adults in

413 those strains ("high" strains) with significantly higher steady-state fractional abundance of
414 mtDNA^{uaDf5} showed significantly greater rates of reduction of the defective mtDNA (reduction
415 from 5.4:1 to 3.3:1 in *atfs-1(et15)*, from an extraordinarily high 6.5:1 to 2.8:1 in *ced-10(n1993),*
416 and from 6.4:1 to 3.3:1 in *ced-13(sv32)*) compared to offspring of ("low" strain) mothers with
417 lower steady-state fractional abundance of the mutant mtDNA (reduction from 4.7:1 to 4.2:1 in
418 WT, from 3.9:1 to 2.8:1 in *ced-3(n2454),* and from 3.2:1 to 2.5:1 in *ced-4(n1162)*). Remarkably,
419 therefore, day 4 progeny from "high" strains actually inherit a *lower* mtDNA^{uaDf5} load than their
420 siblings born from day 1-3 mothers (Fig. 3C, 5A). Indeed, we found a strong correlation (r^2=0.61,
421 $p < 0.001$) between the steady-state level of mtDNA^{uaDf5} in mothers and the capacity for its
422 removal between mother and progeny during day 4 of adulthood (Fig. 5B). These results raise
423 the possibility that very high levels of mtDNA^{uaDf5} in older mothers activate additional mtDNA
424 purifying selection independent of the UPR^{MT} and PCD machinery, thereby ensuring that progeny
425 are not overloaded with defective mitochondria.
426

427 **Discussion**

428 We have obtained several lines of evidence indicating that regulators of PCD and the aging
429 program function in mtDNA quality control and accumulation of defective mtDNA in *C. elegans*.
430 We report eight major findings: 1) regulators of germline PCD are required for effective removal
431 of deleterious mtDNA from the germline; 2) the cell death machinery functions in either a non-
432 canonical cell death pathway or in a non-apoptotic role to mediate mitochondrial purifying
433 selection; 3) the CSP-1 caspase has as strong of an effect on mitochondrial purifying selection as
434 the major PCD regulator CED-3; 4) mtDNA^{uaDf5} progressively accumulates in the germline as
435 adults age; 5) this age-dependent accumulation of mtDNA^{uaDf5} is transmitted to progeny;
436 however, the burden of the defective mtDNA is lower in offspring than mothers suggesting
437 intergenerational purifying selection; 6) two separate aging pathways, the IIS and CLK-1
438 pathways, act synergistically to regulate mtDNA^{uaDf5} levels; longer-lived mutants show reduced
439 levels of the defective mtDNA while shorter-lived mutants show increased levels compared to
440 otherwise wildtype animals; 7) the rate of mtDNA^{uaDf5} accumulation is inversely correlated with
441 lifespan in aging mutants; 8) intergenerational removal of mtDNA^{uaDf5} occurs more effectively
442 during transmission from older mothers with high burden of the defective mtDNA.

443 Previous reports demonstrated that UPR^{MT} limits *uaDf5* clearance, and that eliminating
444 the UPR^{MT}-mediating transcription factor, ATFS-1, lowers mtDNA^{uaDf5} abundance [25,27]. Our
445 identification of a second mutation in the *uaDf5* mutant that results in premature truncation of
446 the ND4 gene product raises the possibility that expression of both the truncated ND4 and the
447 ND1-CYTB fusion protein might together activate UPR^{MT}. The possibility that it is the production

448 of aberrant polypeptides resulting from these mutations that trigger this response will require
449 analysis of additional mtDNA mutants.
450
451 **Mitochondrial deletion mutant *uaDf5* as a model for mitochondrial disease**
452 We found that *uaDf5* affects brood size, embryonic lethality, and developmental rate,
453 highlighting its use as a model for investigating mitochondrial diseases. The reduced brood size
454 in *uaDf5*-bearing animals might reflect diminished germ cell proliferation, as mitochondria have
455 been implicated in progression of germline maturation [93,94]. Alternatively, the defective
456 mtDNA might trigger hyperactivation of the germline PCD pathway that specifically removes
457 germ cells with the highest burden of defective mtDNA, as suggested by our results, resulting in
458 the survival of fewer mature oocytes. The increased embryonic lethality in the *uaDf5* strain may
459 be a consequence of a genetic bottleneck effect, leading to rapid differences in mtDNA allele
460 frequencies [95–97] and a subpopulation of oocytes containing levels of mtDNA^{uaDf5} that exceed
461 a threshold required for viability.
462 We were surprised to find, in contrast to a previous report [98], that mtDNA^{uaDf5} did not
463 alter lifespan. Given that mitochondrial mutations are often coupled with compensatory
464 mutations in the nuclear genome [99–103], one possible explanation for this discrepancy might
465 be that a compensatory nuclear mutation exists in the strain analyzed, diminishing the impact of
466 the defective mitochondrial genome. We note, however, that we backcrossed the *uaDf5* strain
467 extensively to the laboratory reference strain N2 prior to performing the reported analyses. It is
468 conceivable that although we observed no effect in the lab, *uaDf5* might alter lifespan under
469 natural conditions. Exposure to increased stress from growth in the wild might be less tolerated

470 in animals bearing mtDNA^{uaDf5}, as has been observed with other mitochondrial mutants [104],
471 resulting in diminished lifespan.
472
473 **Caspases and cell death machinery regulate mitochondrial purifying selection**
474 Our results lend support to the hypothesis that germline PCD mechanisms may be used
475 to cull germline cells with defective mtDNA (Fig. 6A). Developmentally programmed cell death
476 and cell death in response to genotoxic stress are mediated by caspases upon activation by the
477 *C. elegans* octameric apoptosome which is formed when the inhibition of CED-4 by CED-9 is
478 disrupted through binding of BH-3-only proteins EGL-1 and CED-13 in the soma and germline,
479 respectively. We propose that in response to mitochondrial genotoxic stress (increased
480 mtDNA^{uaDf5} load), caspases CED-3 and CSP-1 are activated by the BH-3 only domain protein CED-
481 13 thereby triggering mitochondrial purifying selection independent of CED-9 and the CED-4
482 apoptosome, either through germ cell PCD or a non-apoptotic role of these caspases (Fig. 6A).
483 Mutations that eliminate the function of caspases that act in PCD result in elevated
484 mtDNA^{uaDf5} levels. Two mutations affecting the p15 domain of the CED-3 caspase result in a
485 significantly increased molar ratio of *uaDf5*, highlighting the importance of the p15 domain in
486 mtDNA quality control. It is noteworthy that the two mutations that result in a more substantial
487 effect on mtDNA^{uaDf5} abundance affect CED-3 structure more dramatically: *ced-3(n717)* results in
488 a splicing error, and *ced-3(n1286)* is a nonsense mutation [54]. In contrast, *ced-3(n2454)*, which
489 results in a subtle (statistically insignificant) increase in mtDNA^{uaDf5}, is a substitution predicted to
490 impart a much weaker effect on the protein structure [54]. The effect of the *ced-3(n718)* allele,
491 which resides in the prodomain of CED-3, suggests that that portion of the protein may act to

492 inhibit mtDNA quality control. Taken together, our results suggest that CED-3 may carry out a
493 specialized activity in mtDNA-activated PCD. We found that a second caspase, CSP-1, which plays
494 a minor role in PCD [56,57], is also required in mtDNA quality control: a *csp-1(-)* knockout
495 mutation results in increased abundance of mtDNA^{uaDf5} and enhances the effect of *ced-3(n717)*,
496 suggesting that CSP-1 may play a larger role in removal of defective mtDNA than it does in other
497 forms of PCD. An exciting possibility is that caspases act in mtDNA quality control via a mechanism
498 that is distinct from their normal action in PCD. Such putative roles for caspases and other
499 mitochondrial factors in non-apoptotic mitochondrial quality control may have been co-opted
500 during metazoan evolution with the innovation of PCD.

501 Analysis of additional PCD components further implicate a role for germline PCD in
502 mitochondrial purifying selection. These include CED-13, the germline-specific PCD effector, and
503 components of the cell corpse engulfment pathway, which activate PCD likely through a complex
504 feedback mechanism that ensures cells destined to die proceed irreversibly through the process
505 [66,67]. In all cases, mutations in these components result in increased mtDNA^{uaDf5} levels. In
506 vertebrates, mitochondrial reactive oxygen species (mtROS) trigger apoptosis via the intrinsic
507 mitochondrial pathway [120]. Interestingly, elevated mtROS promotes longevity that is in part
508 dependent on the core cell death machinery in *C. elegans*, involving CED-9, CED-4, CED-3 and
509 CED-13, but not EGL-1 [105]. In that study, the authors reported that the protective effect of the
510 cell death machinery on lifespan was independent of PCD in the soma; however, germline cell
511 death was not characterized. Given that CED-13, and not EGL-1, is the predominant BH3-domain
512 protein functioning in the germline [58] and that ablation of the germline leads to extended
513 lifespan [106], our findings support the possibility that germline progenitors carrying defective

514 mitochondria selectively undergo PCD, ensuring homeostatic mtDNA copy number and health of
515 progeny.

516 A striking exception to our findings was seen with mutations that eliminate the function
517 of the pro-apoptotic regulator CED-4. Neither the *ced-3(n718)* mutation that disrupts the CED-3
518 CARD domain, which is involved in recruitment to the apoptosome by stabilizing its interaction
519 with CED-4 [44,107], nor two *ced-4(-)* mutations, result in increased accumulation of mtDNA^{uaDf5},
520 suggesting non-canonical, CED-4-independent activation of CED-3 in mitochondrial purifying
521 selection. It is possible that the CARD mutation (G65R) in the *ced-3(n718)* mutant [54] reduces
522 the fraction of CED-3 in complex with the apoptosome, which might release more of the protein
523 for its role in mitochondrial purifying selection. Interestingly, the CARD linker domain has been
524 found to have an inhibitory effect on the pro-caspase-9 zymogen [108]. *ced-3(n718)* could be
525 effectively acting as a gain-of-function allele in the process of purifying selection, reflected by the
526 lower levels of mtDNA^{uaDf5} in this mutant background.

527 It is noteworthy that CED-4 and its mammalian Apaf1 relatives regulate a variety of
528 cellular functions that are unrelated to their activities in PCD. These include cell growth control
529 influenced by DNA damage, centrosomal function and morphology, neuronal regeneration, and
530 inhibition of viral replication [109–112]. In addition, as a result of differential RNA splicing, *ced-4*
531 encodes proteins with opposing activities, generating both an activator and a repressor of
532 apoptosis [113], which further complicates analysis of its action. Thus, it is conceivable that CED-
533 4 might exert opposing effects on purifying selection, reflecting its pleiotropic activities in
534 development and confounding an unambiguous interpretation of its action in this process.

535

536 **IIS and CLK-1 synergistically regulate germline accumulation of mtDNA^{uaDf5} as adults age**

537 We found that most of the increase in the fractional abundance of mtDNA^{uaDf5} as worms
538 age throughout the period of self-fertility (days 1-4) occurs in the germline. However, the relative
539 amount of the defective mtDNA continues to increase in older animals when the germline is no
540 longer actively proliferating [76], suggesting that mtDNA proliferation also occurs in somatic
541 tissues throughout the aging process. This behavior mirrors the dynamics of mutant mtDNAs
542 observed in other organisms, including human, mouse, rat, and rhesus monkey [35,73,79]. While
543 removal of the germline in worms results in extended lifespan [114,115], it is not clear whether,
544 or to what extent, this increased lifespan might be attributable to accumulation of mutant
545 mtDNA, since the lack of germline leads to a variety of cellular responses [116,117], any of which
546 might lead to lifespan extension.

547 These studies do not reveal whether, or how, aging and accumulation of defective mtDNA
548 are causally linked. However, our findings that steady-state levels of mtDNA^{uaDf5} are lowered in
549 long-lived mutants (*daf-2* (IIS pathway; [28]) and *clk-1* (mitochondrial function; [118,119])) and
550 that rates of its accumulation are strongly inversely correlated with lifespan extension through
551 independent pathways, suggests that mtDNA purifying selection mechanisms are influenced by
552 aging programs (Fig. 6A). Further bolstering this potential link is our finding that short-lived
553 mutants (*daf-16* and *aak-2,* both involved in the IIS pathway [28]), show higher steady-state levels
554 of mtDNA^{uaDf5}. That this effect is greater in *aak-2* mutants than in *daf-16* mutants suggests that
555 the AAK-2 branch of the IIS pathway influences mtDNA quality control more significantly than
556 does the DAF-16 branch. One of the substrates of AAK-2 is SKN-1/Nrf2, a multifaceted
557 transcription factor with roles in stress response and longevity, and one of its isoforms, SKN-1a,

558 localizes to the mitochondrial surface [120], raising the possibility that AAK-2 might influence
559 clearance of defective mtDNA through SKN-1 action. It will be of interest to assess how defective
560 mtDNA might coordinately trigger quality control and stress-response pathways.

561 Our observation that IIS pathway components and CLK-1 act synergistically on the mtDNA
562 quality control machinery raises the possibility that these two distinct lifespan-regulating
563 pathways converge on a common system for removal of defective mtDNA, such as a global
564 mitochondrial stress response pathway. Candidates for mediating this removal process include
565 mitochondrial fission/fusion [17,20,121], mitophagy [18,19,122], and the UPR^{MT} [22–27], all of
566 which are known to act in mtDNA quality control, as well as modulation of the regulatory
567 pathway for PCD, as suggested by our findings.

568

569 **PCD is uncoupled from aging during intergenerational mitochondrial purifying selection in**
570 **older mothers**

571 Analysis of newly hatched L1 larvae revealed that the relative load of $mtDNA^{uaDf5}$ is
572 transmitted from mother to offspring, with evidence for intergenerational purifying selection
573 (Fig. 6B). This finding implies that mtDNA quality control occurs between germline stem cell
574 expansion in the mature female germline and L1 hatching, a developmental period that spans
575 many potential stages at which it might occur, including germline PCD, oocyte maturation, and
576 the entirety of embryogenesis. It is conceivable that this selection process acts at multiple stages
577 throughout this developmental window and that the decreased burden of defective mtDNA in
578 newly hatched L1 larvae reflect the summation of a series of sequentially acting processes that
579 incrementally enrich for healthy mtDNA.

580 The efficacy of intergenerational removal of mtDNA^{uaDf5} increases in old mothers,
581 including in strains lacking pro-apoptotic regulators. The clearance is particularly precipitous in
582 strains with a very high burden of defective mtDNA as seen in the absence of CED-13, CED-10,
583 and ATFS-1, suggesting a critical threshold beyond which a germline PCD-independent mtDNA
584 quality control process may be triggered in these older mothers (Fig. 6B). One possible
585 explanation for this observation is that an mtDNA purifying selection mechanism that is typically
586 inhibited by germline PCD might be activated in older mothers. This hypothesized purifying
587 selection mechanism might be triggered by the unique cellular environment associated with
588 aging such as increased organelle or macromolecule damage. Alternatively, the effect might be
589 the result of an age-dependent genetic program.

590 While our study has uncovered new mechanisms acting in mtDNA purifying selection and
591 its relationship to aging, it is of note that some level of mtDNA^{uaDf5} is maintained in all but the
592 most extreme conditions we have observed (e.g., in the *daf-2(e1391) clk-1(qm30)* double
593 mutant, in which the defective mtDNA is extirpated). This finding raises the possibility that
594 some degree of heteroplasmy, even with defective mtDNA, is not only tolerated, but may be
595 adaptive by providing a degree of evolutionary plasticity. Cells might purposefully allow for
596 limited heteroplasmy as a way of increasing genetic heterogeneity that might prove
597 evolutionarily advantageous. Such heterogeneity may also be essential to allow mtDNA to co-
598 evolve with changes arising in the nuclear genome. It may be that a dynamic balance between
599 active mtDNA purifying selection, including the mechanisms identified here, and the
600 permissibility of limited heteroplasmy, is modulated according to environmental or
601 physiological demands.

602 **Materials and Methods**
603
604 **Culturing of nematodes**

605 Nematode strains were maintained on NGM plates as previously described at either 20°C
606 or 15°C for the temperature-sensitive strains [123]. Supplementary Tables 1, 2 and 3 provide
607 details of all strains used in this study. Strains without a JR designation were either provided by
608 the CGC which is funded by NIH Office of Research Infrastructure Programs (P40 OD010440) or
609 were obtained from the Mitani lab (strains with a FX designation or JR strains containing alleles
610 with a tm designation were generated from Mitani lab strains) [124].

611 **Population collection by age**

612 Upon retrieval of a stock plate for a given strain, three chunks were taken from the stock
613 plate and placed onto three separate large NGM plates to create three biological replicates
614 ("lines"). Each of these lines was chunked approximately each generation to fresh large NGM
615 plates (every 3 days if maintained at 20°C or 25°C, or every four days if maintained at 15°C, being
616 careful to not let the worms starve between chunks). After four generations of chunks, an egg
617 prep was performed on each line (as described previously; [123]) and left to spin in M9 overnight
618 to synchronize the hatched L1s. The next day, each egg prep was plated onto three large seeded
619 plates at an equal density and the worms were left to grow to day 2 adults (second day of egg
620 laying). The day 2 adult worms were egg prepped for synchronization and left to spin in M9 buffer
621 overnight. The next day, each egg prep was plated onto five large NGM plates at equal density.
622 Once the worms reached day 1 of adulthood (first day of egg-laying), one of the plates was used
623 to collect 200 adult worms by picking into 400 µl of lysis buffer, and the remaining adults on the
624 plate were egg prepped for the collection of hatched L1 larvae in 400 µl lysis buffer the following

625 day. The worms on the four remaining plates were transferred to a 40 µm nylon mesh filter in
626 order to separate the adults from the progeny, and the resulting adults were resuspended in M9
627 and pipetted onto fresh large NGM plates. This process was repeated for the following three days
628 (Day 2-4 of adulthood). Day 5-10 adults were moved to fresh NGM plates every 2nd day using a
629 40 µm nylon mesh filter, and the resulting day 10 adults were collected in lysis buffer.

630 **ddPCR**

631 The worm lysates were incubated at 65°C for 4 hours and then 95°C for 30 minutes to
632 deactivate the proteinase K. Each lysate was diluted; 100-fold for 200 worm adult population
633 lyses, 2-fold for 200 worm L1 population lyses, and 25-fold for individual adult lyses. 2 µl of the
634 diluted lysate was then added to 23 µl of the ddPCR reaction mixture, which contained a
635 primer/probe mixture and the ddPCR probe supermix with no dUTP. The primers used were:

636 WTF: 5'-GAGGGCCAACTATTGTTAC-3'

637 WTR: 5'-TGGAACAATATGAACTGGC-3'

638 UADF5F: 5'-CAACTTTAATTAGCGGTATCG-3'

639 UADF5R: 5'-TTCTACAGTGCATTGACCTA-3'

640 The probes used were:

641 WT: 5'-HEX-TTGCCGTGAGCTATTCTAGTTATTG-Iowa Black® FQ-3'

642 UADF5: 5'-FAM-CCATCCGTGCTAGAAGACAAAG- Iowa Black® FQ-3'

643 The ddPCR reactions were put on the BioRad droplet generator and the resulting droplet-
644 containing ddPCR mixtures were run on a BioRad thermocycler with the following cycle
645 parameters, with a ramp rate of 2°C/sec for each step:

646 1. 95°C for 5 minutes

647 2. 95°C for 30 seconds

648 3. 60°C for 2 minutes

649 4. Repeat steps 2 and 3 40x

650 5. 4°C for 5 minutes

651 6. 90°C for 5 minutes

652 After thermocycling, the ddPCR reaction plate was transferred to the BioRad droplet reader and
653 the Quantasoft software was used to calculate the concentration of mtDNA^{uaDf5} (FAM positive
654 droplets) and mtDNA^{WT} (HEX positive droplets) in each well.

655 **Lifespan analysis**

656 Confluent large plates were egg prepped and left to spin in M9 overnight for
657 synchronization. The hatched L1s were plated onto large thick plates and allowed to grow to day
658 2 adults before being egg prepped a second time and left to spin in M9 overnight. The next
659 morning, referred to as day 1 for lifespan determination, L1s were singled out onto small plates.
660 Once the worms started laying eggs, they were transferred each day to a fresh small plate until
661 egg laying ceased, after which the worms remained on the same plate unless bacterial
662 contamination required transfer to a fresh plate. Worms were considered dead if there was no
663 movement after being lightly prodded with a worm pick. Worms that died due to desiccation on
664 the side of the plate were excluded from analysis.

665 **Brood size and embryonic lethality analysis**

666 Confluent large plates were egg prepped and left to spin in M9 overnight for
667 synchronization. The hatched L1s were plated onto large thick plates and allowed to grow to day
668 2 adults before being egg prepped a second time and left to spin in M9 overnight. The next

669 morning, L1s were singled out onto small plates. Once the worms started laying eggs, they were
670 transferred each day to a fresh small plate until egg laying ceased. The day after transfer to a
671 fresh plate, unhatched embryos and hatched larvae on the plate from the previous day were
672 counted. This was done for each of the days of laying and the total of unhatched embryos and
673 hatched larvae from all plates from a single worm were tabulated to determine total brood size.
674 To determine embryonic lethality, the total number of unhatched embryos was divided by the
675 total brood size. Worms that died due to desiccation on the side of the plate were excluded from
676 analysis.

677 **Developmental time course analysis**

678 Confluent large plates were egg prepped and left to spin in M9 overnight for
679 synchronization. The hatched L1s were plated onto large thick plates and allowed to grow to day
680 2 adults before being egg prepped a second time and left to spin in M9 overnight. The next
681 morning, L1s were singled out onto small plates. The stage of the worms was assayed every 12
682 hours for the first 72 hours after plating. For determining the stage at 60 hours, L4 worms were
683 divided up into three subgroups based on morphology: young-L4, mid-L4, and late-L4; otherwise,
684 all other staged worms were not divided up into subgroups. Worms that died due to desiccation
685 on the side of the plate were excluded from analysis.

686 **Genotyping the *w47* allele**

687 DNA was collected from reference strain (N2) and two *uaDf5*-containing strains, LB138
688 and JR3630. Mitochondrial DNA was extracted and the DNA libraries were prepared using
689 Nextera Kit and then sequenced using an Illumina NextSeq500. Prior to alignment, reads from
690 fastq files were trimmed using Trimmomatic. Trimmed, pair-end reads (2x150) were then

691 mapped to the *C. elegans* assembly reference sequence WBcel235 using Burrows-Wheeler
692 Aligner (BWA) [125]. Picard Tools (http://broadinstitute.github.io/picard/) was used to mark
693 duplicate reads, and SAMtools [126] was used to merge, index and create pile-up format. VarScan
694 [127] was used to call variants, and only variants with minimum coverage of 100 and a minimum
695 variant frequency call of 0.01 were considered for analysis.

696 **Statistical Analysis**

697 Summary statistics, ANOVA, Mann-Whitney tests, and linear regression were calculated
698 using R v3.4.1. The details of the statistical tests are reported in the figure legends.

699

700 **Figures**

701 **Figure 1**

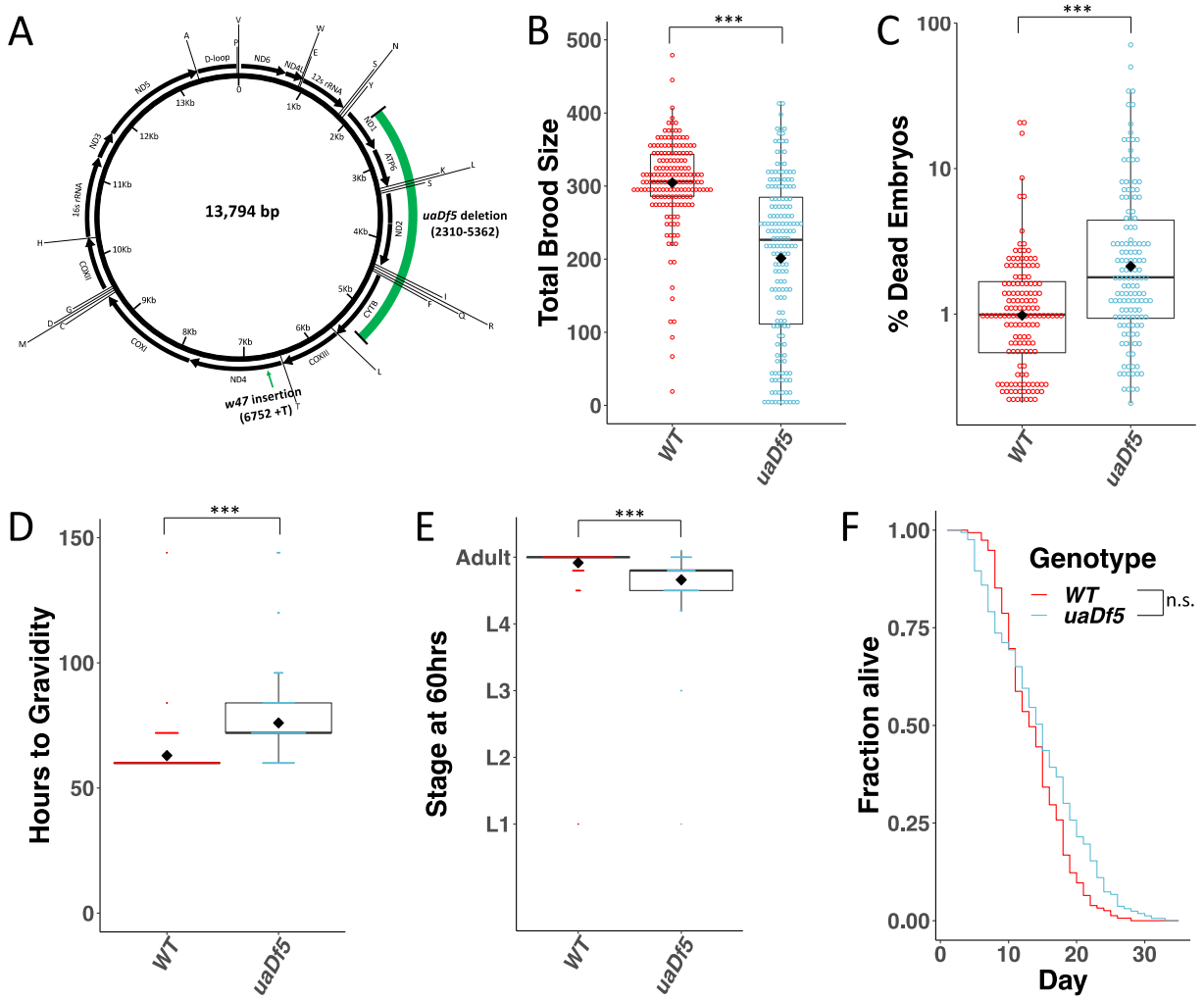

702

703 **Figure 1: Analysis of the impact of mtDNA^{uaDf5} on fitness parameters. (A)** Diagram of *C. elegans*

704 mtDNA. Black bars with arrows indicate the locations of genes and direction of transcription.

705 Black lines with letters indicate the locations of tRNAs. Green bars show the locations of the

706 mtDNA^{uaDf5} deletion as well as the linked *w47* insertion that was identified via Illumina

707 sequencing. **(B)** Brood size analysis of mtDNA^{uaDf5} compared to laboratory wildtype N2. **(C)**

708 Embryonic lethality analysis of *uaDf5* compared to laboratory wildtype N2. **(D)** Developmental

709 rate analysis of mtDNA^{uaDf5} compared to laboratory wildtype N2, counting how many hours it

takes for starved L1s to reach gravidity once plated on food. **(E)** Developmental rate analysis of mtDNA^{uaDf5} compared to laboratory wildtype N2, staging worms 60 hours after synchronized, staved L1s are plated on food. **(F)** Survival curve analysis of mtDNA^{uaDf5} compared to laboratory wildtype N2, day 1 is defined as the day starved L1s are plated on food. Median lifespan and statistics are presented in Supplemental Figure 2. For **B-E**, box plots show median and IQR, and the diamond indicates the mean. Statistical analysis was performed using the Mann-Whitney test. (*** $p < 0.001$, n.s. not significant).

718 **Figure 2**

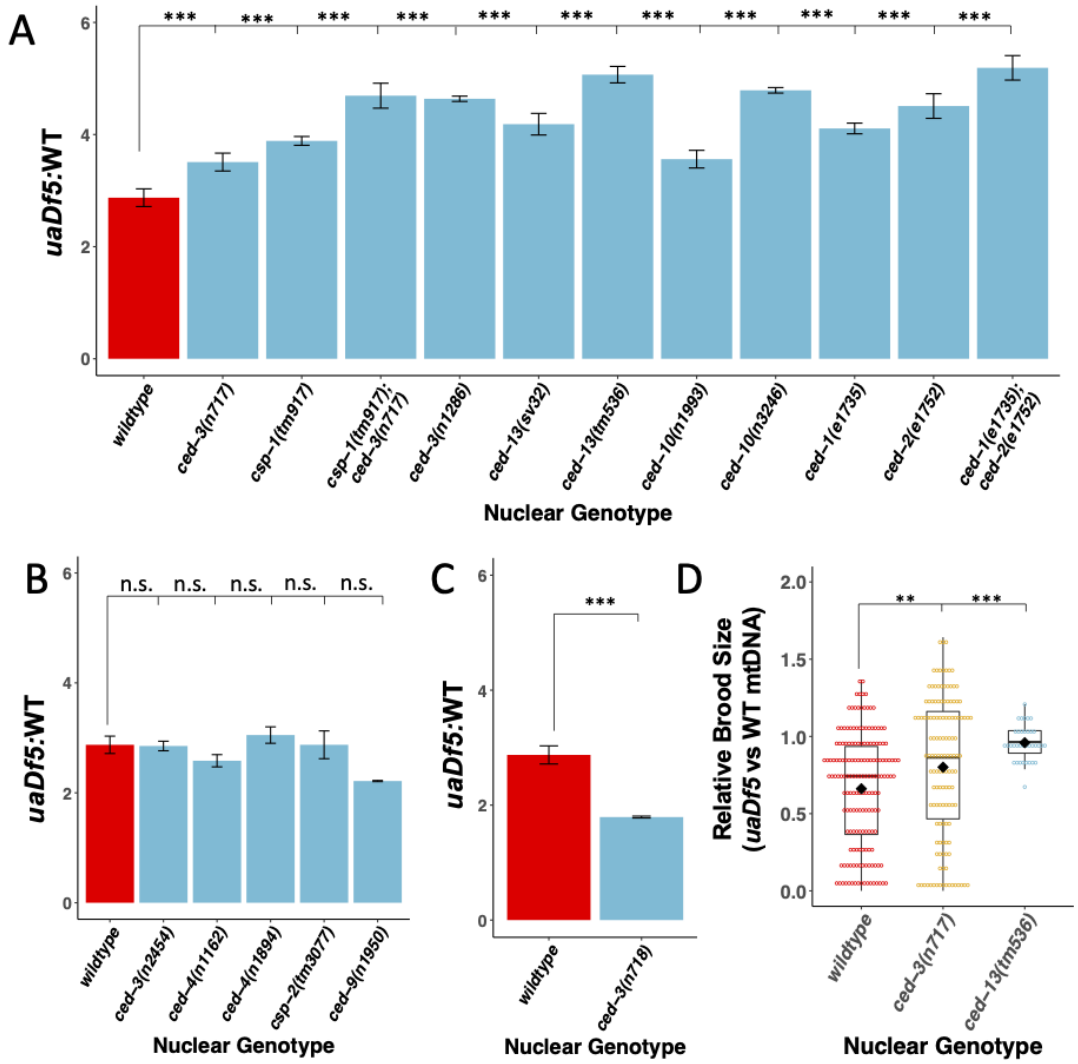

719
720

721 **Figure 2: Regulators of PCD act on mutant mtDNA. (A-C)** ddPCR analysis of the steady-state

722 molar ratio of mtDNA^{uaDf5} in 200 worm populations of day 1 adults of various PCD mutant

723 backgrounds. **(A)** PCD mutants that result in a significant increase in the molar ratio of

724 mtDNA^{uaDf5}. **(B)** PCD mutants that result in no statistical change in the molar ratio of mtDNA^{uaDf5}.

725 **(C)** PCD mutant that results in a significant decrease in the molar ratio of mtDNA^{uaDf5}. **(D)** The

726 relative brood size of the animals with and without mtDNA^{uaDf5} in the indicated mutant

727 backgrounds. For each nuclear genotype shown, the brood size of *uaDf5*-containing worms was

728 normalized by dividing by the average brood size of worms containing only *WT-mtDNA*. Box plots
729 show the median and IQR, the diamond indicates the mean. For **A-C**, n=3 or more biological
730 replicates of 200 worm populations were performed for each genotype. Statistical analysis was
731 performed using one-way ANOVA with Dunnett's correction for multiple comparisons. For **D**,
732 statistical analysis was performed using the Mann-Whitney test. Error bars represent SEM. (***
733 $p < 0.001$, ** $p < 0.01$, * $p < 0.05$, . $p < 0.1$, n.s. not significant).
734

735 **Figure 3**

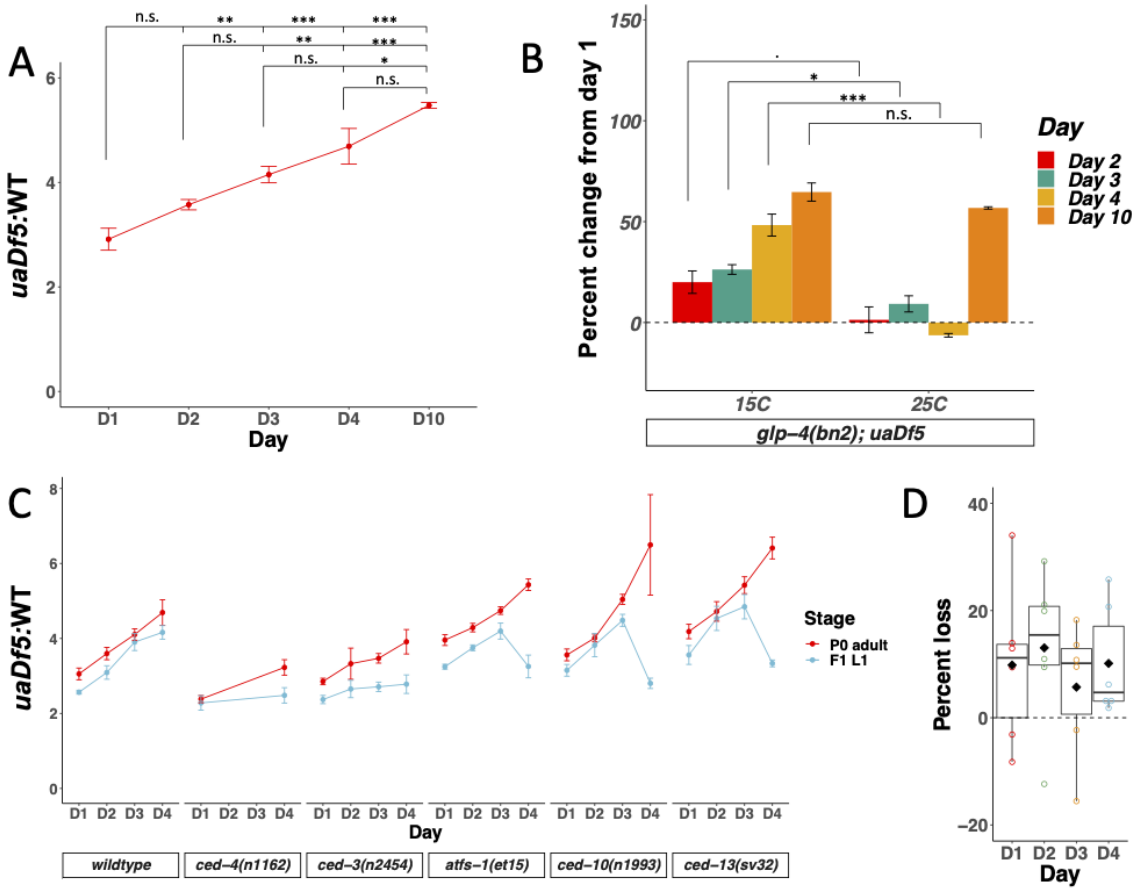

736

737 **Figure 3: mtDNA^{uaDf5} accumulates in the germline of aging adults, and evidence of purifying**

738 **selection between mother and offspring. (A)** Analysis of the molar ratio of mtDNA^{uaDf5} in aging

739 adults in a wildtype nuclear background. **(B)** Analysis of the percent change of *uaDf5:*WT from

740 day 1 (Y axis = (*uaDf5:*WT day x -*uaDf5:*WT day 1)/(*uaDf5:*WT day 1)). For *glp-1(q231ts), fem-*

741 *3(q20ts),* and *glp-4(bn2ts),* 15°C is the permissive temperature (germline development occurs)

742 and 25°C is the restrictive temperature (female germline development is inhibited). Statistical

743 analysis was performed using one-way ANOVA with Tukey correction for multiple comparisons.

744 (*** $p < 0.001$, ** $p < 0.01$, * $p < 0.05$, . $p < 0.1$). Error bars represent SEM. **(C)** Analysis of the

745 molar ratio of mtDNA^{uaDf5} in aging adults (P0 adult) and their L1 progeny (F1 L1) in various nuclear

746 backgrounds shows that all strains decrease the *uaDf5* load during transmission from mother to

747 offspring, and that strains with significantly higher mtDNA^{uaDf5} levels (*atfs-1(et15), ced-*
748 *10(n1993)*, and *ced-13(sv32)*) have a more significant removal mechanism at day 4 of adulthood.
749 n=3 or more replicates of 200 worm populations were performed for each timepoint. Error bars
750 represent SEM. Grey dashed line indicates a hypothetical threshold at which high mtDNA^{uaDf5}
751 burden activates enhanced intergenerational purifying selection in older mothers. **(D)** Analysis
752 of the measured loss of mtDNA^{uaDf5} between mother and offspring at each day of adulthood
753 shows that mtDNA^{uaDf5} removal occurs. n=6 replicates of 200 worm populations for each
754 condition.
755

Figure 4

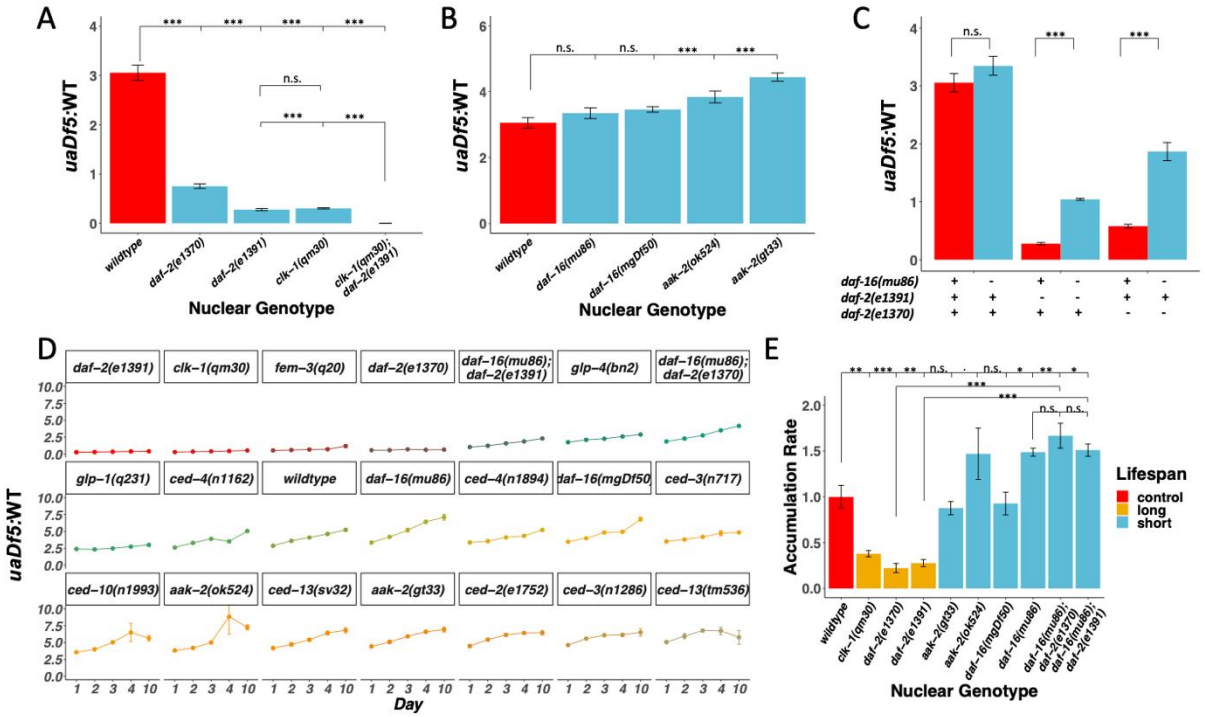

Figure 4: Lifespan mutants have both a lower steady-state level and accumulation rate of mtDNA^{uaDf5}. (A-C) Analysis of molar ratio of mtDNA^{uaDf5} in day 1 adults of various mutant backgrounds. **(A)** Analysis of steady-state mtDNA^{uaDf5} levels in long-lived mutants. **(B)** Analysis of steady-state mtDNA^{uaDf5} levels in short-lived mutants, showing synergistic activity on mtDNA^{uaDf5} removal capacity in the *daf-2(e1391) clk-1(qm30)* double mutant. **(C)** Analysis of steady-state mtDNA^{uaDf5} levels in *daf-2(-)* single and *daf-16(-); daf-2(-)* double mutants, showing a partial rescue of *daf-2(-)* phenotype by *daf-16(-)*. **(D)** Analysis of the molar ratio of mtDNA^{uaDf5} in aging adults in 21 different nuclear backgrounds shows a consistent accumulation trend. **(E)** Summary of the rate of increase for the lifespan regulation mutants, showing that *daf-16* rescues the *daf-2* accumulation rate phenotype. The normalized accumulation rate was calculated by fitting a regression line for each trial and then dividing the slope of the regression line by the slope of the averaged regression line found in a wildtype background. For **all**, n=3 or more replicates of 200

770 worm populations for each genotype and stage. For **A and E,** statistical analysis was performed
771 using one-way ANOVA with Tukey correction for multiple comparisons. For **C**, statistical analysis
772 was performed using one-way ANOVA. For **B**, statistical analysis was performed using one-way
773 ANOVA with Dunnett's correction for multiple comparisons. Error bars represent SEM. (*** $p < 0.001$, ** $p < 0.01$, * $p < 0.05$, . $p < 0.1$, n.s. not significant).
774
775

776 **Figure 5**

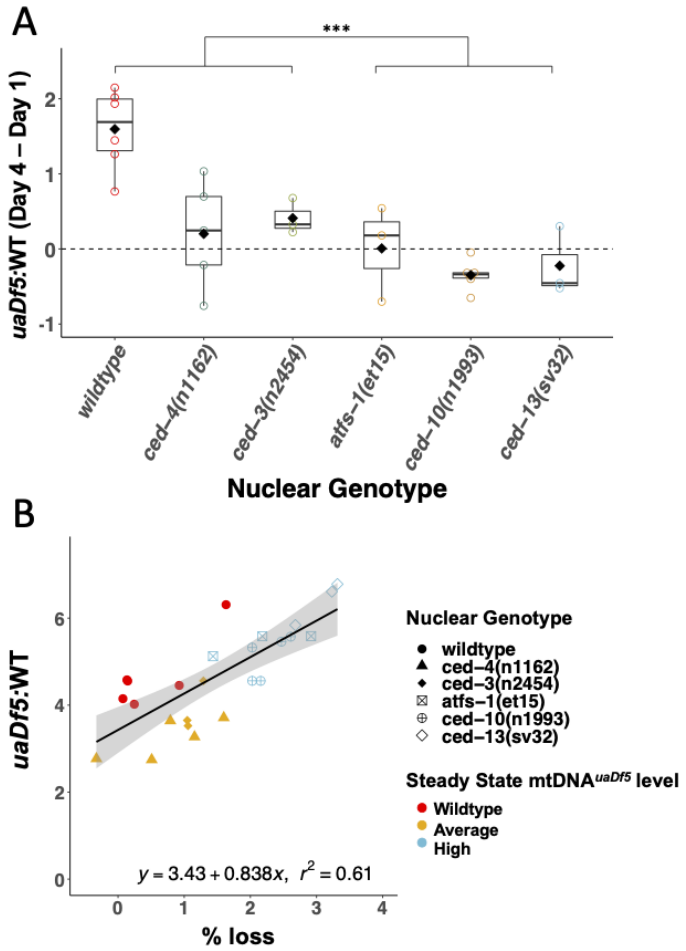

777
778 **Figure 5: Evidence for late adulthood-specific mechanisms for removal of mtDNA^{uaDf5}**

779 **(A)** Subtracting *uaDf5:*WT in progeny from day 1 adults from progeny of day 4 adults shows that
780 day 4 F1-L1s tend to have higher mtDNA^{uaDf5} burden than their day 1 siblings, but this is no longer
781 the case in nuclear backgrounds that result in a significantly higher steady-state levels of
782 mtDNA^{uaDf5} in the adult. n=3 or more replicates for each genotype and statistical analysis was
783 performed using the Mann-Whitney test. **(B)** Comparison of the molar ratio of mtDNA^{uaDf5} in day
784 4 adult mothers to the absolute % removal of mtDNA^{uaDf5} from mother to offspring shows a
785 positive correlation. (*** $p < 0.001$).

786
787

788 **Figure 6**

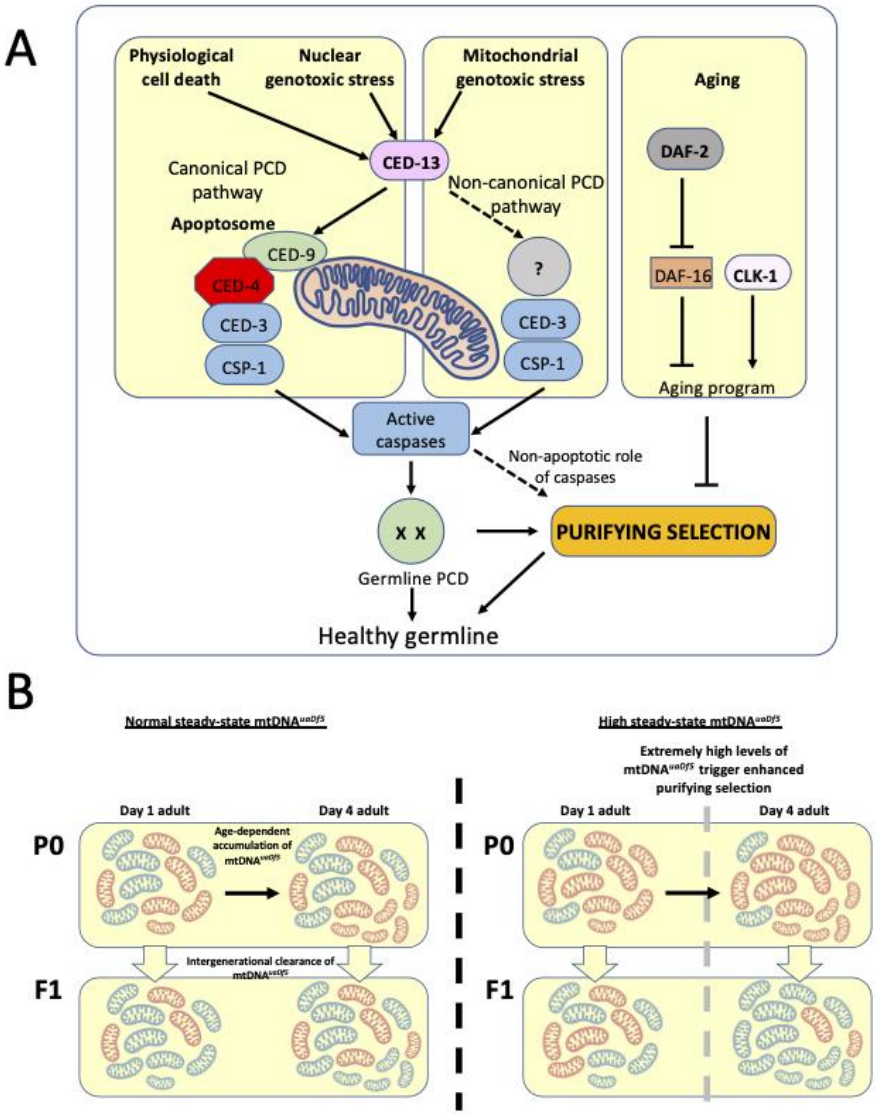

789

790 **Figure 6: Regulation of mtDNA^{uaDf5} accumulation and transmission by the PCD and aging**

791 **pathways**

792 **(A)** Our results suggest that CED-3 and CSP-1, which are activated by BH-3 only protein CED-13,

793 function cooperatively to promote mitochondrial purifying selection, independent of CED-9 and

794 the CED-4 apoptosome. The clearance of mtDNA^{uaDf5} may therefore involve induction of a non-

795 canonical germline PCD mechanism or non-apoptotic action of the CED-13/caspase axis.

796 Additionally, IIS and CLK-1 aging pathways act synergistically to regulate mitochondrial purifying

797 selection**. (B)** mtDNA^{uaDf5} (red) accumulates in the germline relative to mtDNA^{WT} (blue) as adults

798 age and the increased mtDNA^{uaDf5} levels are transmitted to the progeny, although the mtDNA^{uaDf5}

799 burden is consistently lower in progeny than mothers. This intergenerational purifying selection

800 is enhanced in the older mothers of mutants with high steady-state mtDNA^{uaDf5} (e.g., *ced-13*, *ced-*

801 *10,* and *atfs-1*), suggesting a threshold beyond which a germline PCD-independent mtDNA quality

802 control process may be initiated or enhanced in these older mothers.

803 **Supplemental Materials**

804 **Supplemental Figure 1**

A

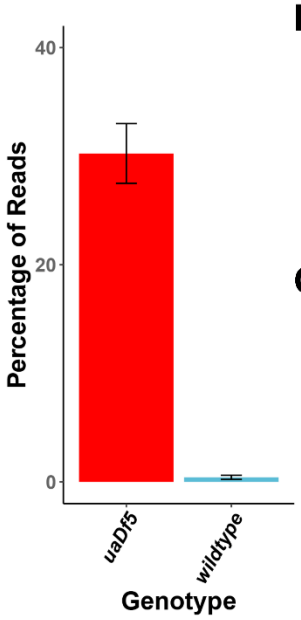

B

Sample	Allele	Total reads	Variant reads	% variant
A	*uaDf5*	858.40*	658.48*	76.71
	w47	631	472	72.62
B	*uaDf5*	451.54*	347.51*	76.96
	w47	339	248	71.06

C

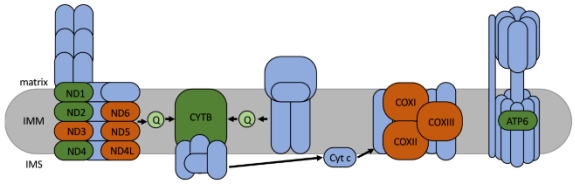

Complex:	I	II	III	IV	V
nDNA-encoded	~30	~8	4	~6	~13
mtDNA-encoded	7	1	0	3	1

D

ND4 (wildtype)

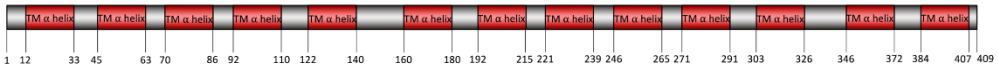

ND4 (*w47*)

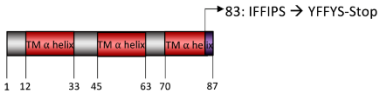

E

ND1 (wildtype)

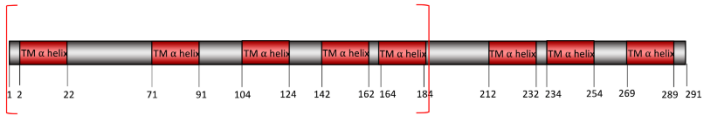

CYTB (wildtype)

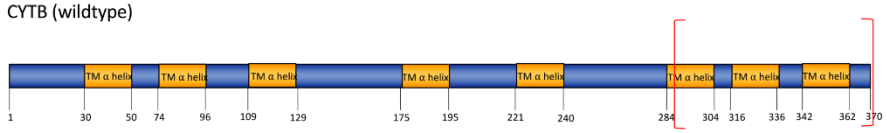

ND1-CYTB (*uaDf5*)

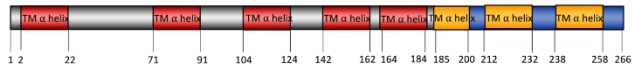

805

806 **Supplemental Figure 1: Characterization of the *uaDf5* allele. (A)** The percentage of reads that
807 mapped to the *w47* insertion in *uaDf5* samples (red) and wildtype samples (blue). Error bars
808 represent SEM. **(B)** Table outlining the percentage of reads that mapped to the *w47* and *uaDf5*
809 mutations in *uaDf5* samples. The number of variant reads was determined by averaging the
810 mapped reads across the deleted region and subtracting that from the average number of reads
811 mapped to the rest of the mtDNA genome (total reads). **(C)** Diagram showing the mitochondrial
812 respiratory chain (MRC) machinery subunits. Blue indicates nDNA-encoded subunits, orange and
813 green indicate mtDNA-encoded subunits. Green indicates those subunits that are knocked out in
814 the *uaDf5* allele (including ND4 which is knocked out by the linked *w47* mutation). **(D)** Diagram
815 showing the likely effect of the *w47* mutation on ND4 protein translation. ND4 is a 409-aa long
816 transmembrane subunit that spans the inner mitochondrial membrane 13 times. The *w47*
817 mutation results in a premature stop codon at position 89, eliminating 10 of the 13 alpha-helix
818 membrane domains. **(E)** Diagram showing the likely effect of the *uaDf5* mutation on ND1 protein
819 translation. ND1 is a 291-aa long transmembrane subunit that spans the inner mitochondrial
820 membrane 8 times and CYTB is a 370-aa long transmembrane subunit that spans the inner
821 mitochondrial membrane 8 times. The *uaDf5* mutation results in a 266 amino acid long fusion
822 protein that connects the first 185 amino acids (and 5 subunits) of ND1 with the last 81 amino
823 acids (and 3 subunits) of CYTB.
824

825 **Supplemental Figure 2**

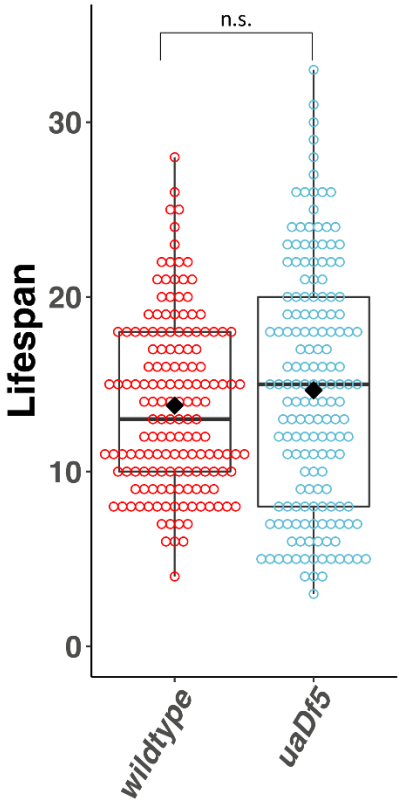

826

827 **Supplemental Figure 2: Lifespan analysis of the impact of *uaDf5*.** Lifespan analysis of N2 bearing

828 *uaDf5* compared to wildtype N2. Day 1 is defined as the day starved L1s are plated on food. Box

829 plots show median and IQR, and the diamond indicates the mean. Statistical analysis was

830 performed using the Mann-Whitney test. (n.s. not significant).

831

832 **Supplemental Figure 3**

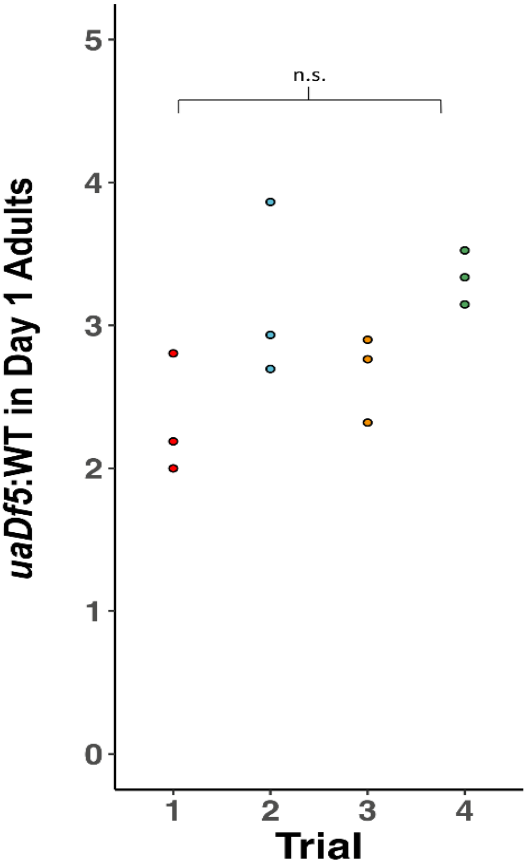

833

834 **Supplemental Figure 3: Reproducibility of ddPCR measurement of *uaDf5*.** Analysis of the steady-
835 state of *uaDf5* in a wildtype nuclear background shows highly stable steady-state levels. Trials
836 were done months apart on different thaws. Dots represent biological replicates. Statistical
837 analysis was performed using one-way ANOVA with Tukey correction for multiple comparisons.
838 (n.s. not significant).

839

840 **Supplemental Figure 4**

A

Allele	Location	Domain	Level of *uaDf5*
n1286	W428opal	p15	highest
n717	Position 403 - Exon 7 acceptor	p15	high
n2454	A466T	p15	unchanged
n718	G65R	Prodomain	low

B

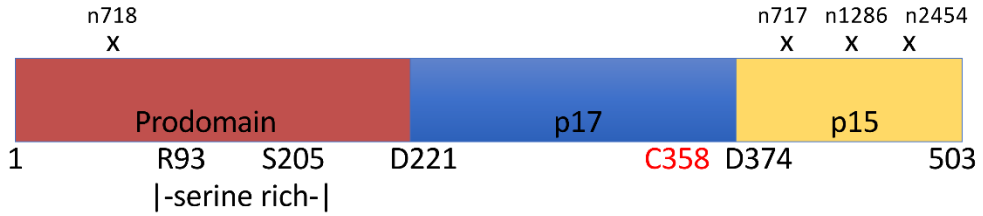

841

842 **Supplemental Figure 4: Analysis of the *ced-3* alleles. (A)** Locations and consequences of the four

843 tested *ced-3* alleles, as well as the measured fractional abundance of *uaDf5*. **(B)** Diagram showing

844 the locations of the mutations for each allele.

845

846 **Supplemental Figure 5**

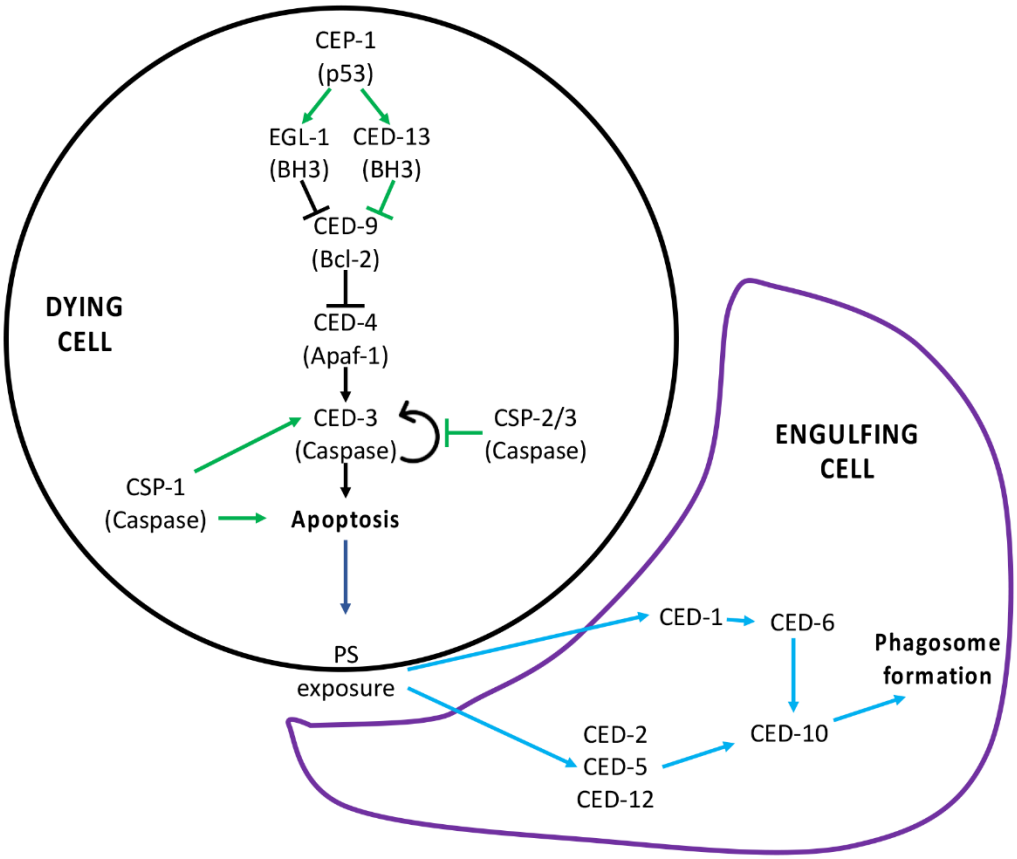

847

848

849 **Supplemental Figure 5: PCD Signaling pathway. (A)** Signaling pathway for programmed cell

850 death. The canonical pathway is shown with black arrows, the noncanonical pathway is shown

851 with green arrows, and the downstream engulfment pathway is shown with blue arrows.

852 Adapted from [38].

853

854 **Supplemental Figure 6**

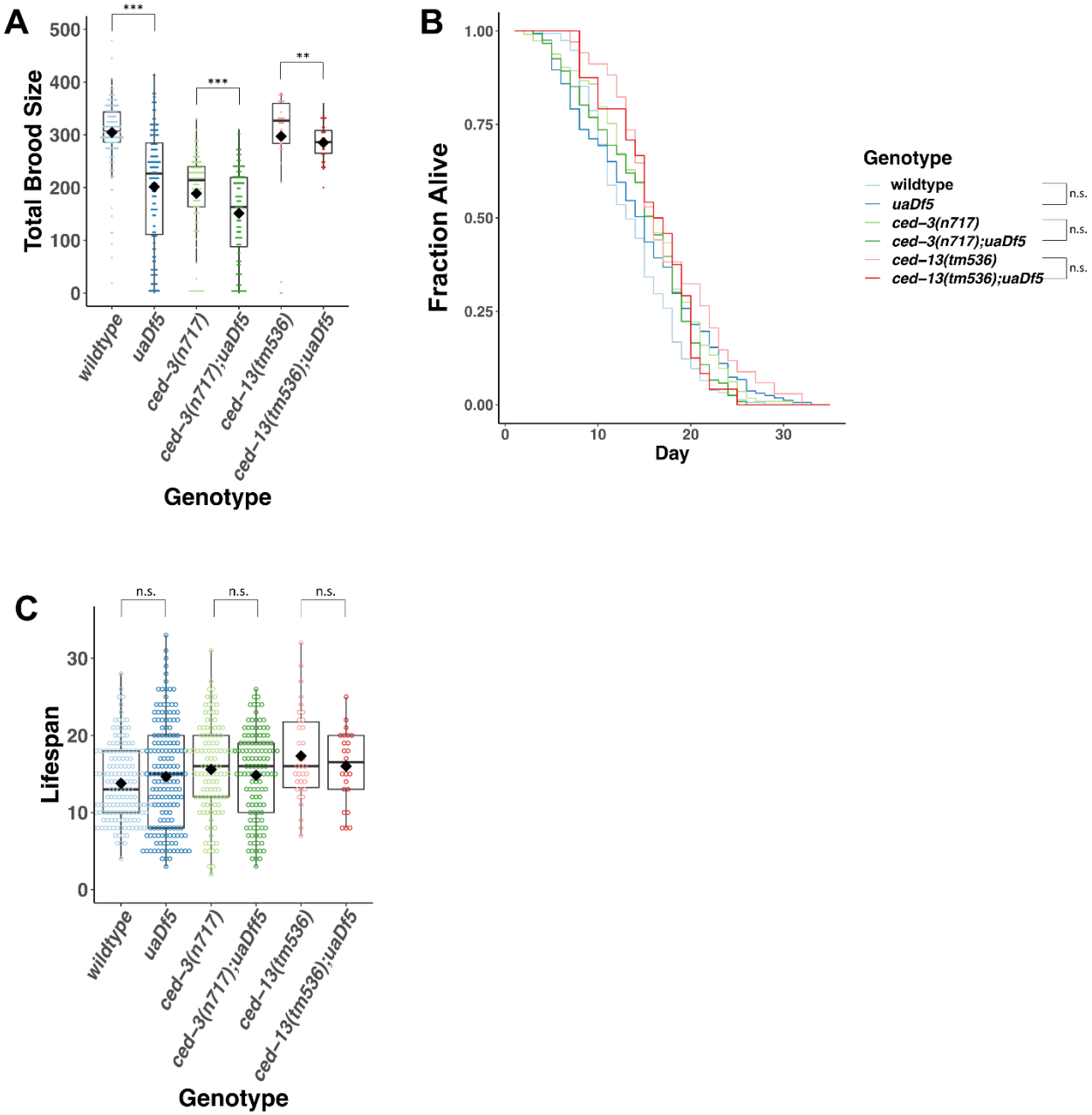

855

856 **Supplemental Figure 6: Analysis of the impact of *uaDf5* on fitness parameters in PCD mutants.**

857 **(A)** Brood size analysis of PCD mutants. **(B)** Lifespan analysis shows that *uaDf5* does not affect

858 lifespan in both wildtype background and in PCD mutant backgrounds. **(C)** Lifespan analysis

859 shows that *uaDf5* does not affect lifespan in a wildtype nuclear background nor in PCD mutant

860 backgrounds. For **B and C,** day 1 is defined as the day starved L1s are plated on food. For **A and**

861 **C**, box plots show median and IQR, and the diamond indicates the mean. Statistical analysis was

862 performed using the Mann-Whitney Wilcoxon test. (*** $p < 0.001$, ** $p < 0.01$, * $p < 0.05$, . $p <$

863 0.1, n.s. not significant).

864

865

866 **Supplemental Figure 7**

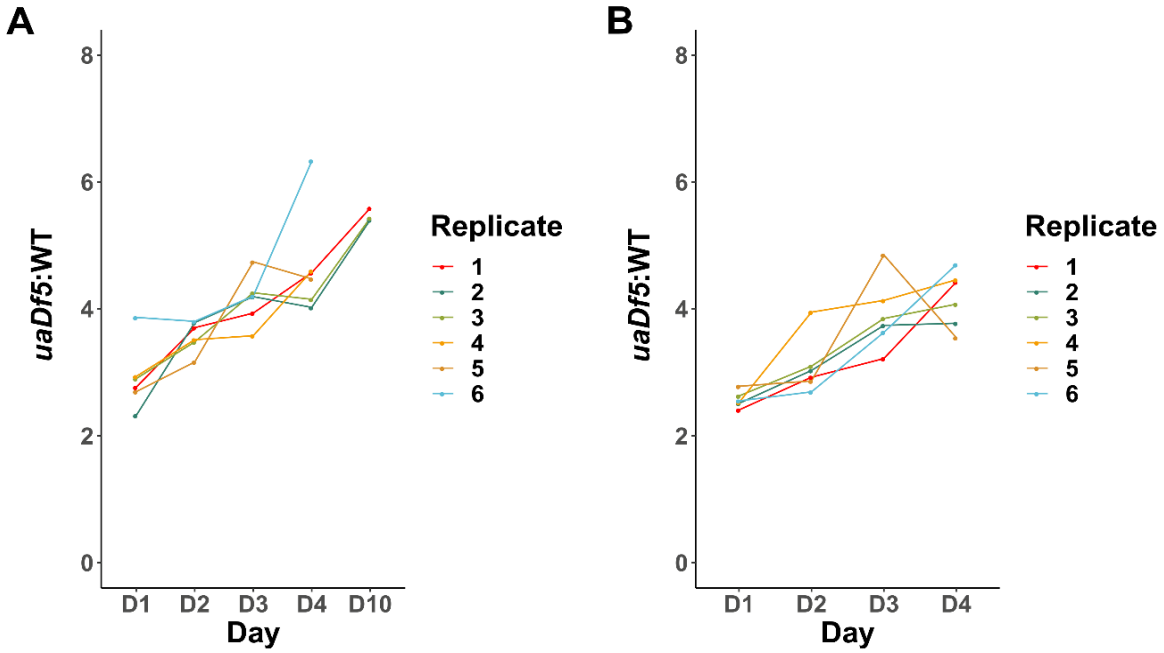

867

868 **Supplemental Figure 7: *uaDf5* accumulation in individual lines of adults and progeny. (A)**
869 Analysis of *uaDf5* accumulation in individual lines of aging P0 adults shows a consistent
870 accumulation trend as adults age. **(B)** Analysis of *uaDf5* accumulation in individual lines of F1-L1
871 progeny that were born from those mothers shown in panel A show a consistent trend of progeny
872 born from older mothers inheriting a larger *uaDf5* load than their siblings born from younger
873 mothers.

874

875 **Supplemental Figure 8**

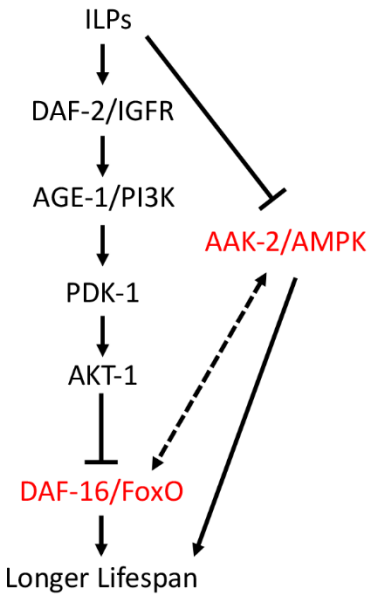

876

877 **Supplemental Figure 8: IIS Signaling pathway.** Insulin-like peptides (ILPs) bind to DAF-2 and
878 activate the PI3P pathway which prevents nuclear translocation of DAF-16. AAK-2 may
879 phosphorylate and activate DAF-16 transcriptional activity. Loss of *aak-2* or *daf-2* (highlighted in
880 red) reduces lifespan

881

882 **Supplemental Figure 9**

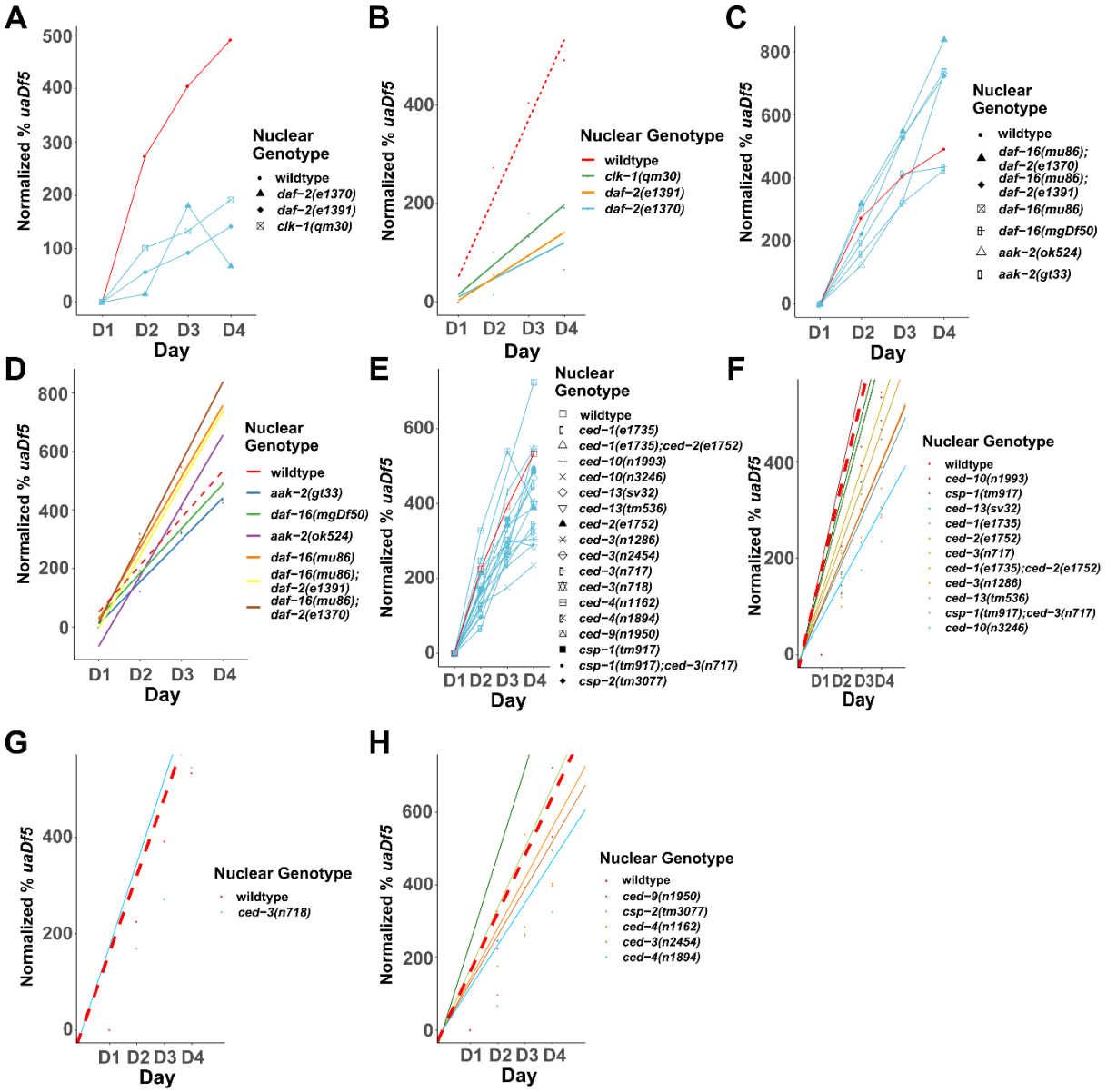

883

884 **Supplemental Figure 9: Analysis of the accumulation of mtDNA^{uaDf5} in PCD and lifespan**

885 **mutants.** Analysis of the normalized fractional abundance *uaDf5* [(% *uaDf5* day x- % *uaDf5* day

886 1)* % *uaDf5* day 1] in steady-state populations, showing the accumulation rate of mtDNA^{uaDf5} as

887 worms age from day 1 to day 4 of adulthood. **(A)** Analysis of the accumulation of *uaDf5* in long-

888 lived mutants. **(B)** Analysis of the accumulation of mtDNA^{uaDf5} in short-lived mutants. **(C-D)** Linear

889 regression analysis of the normalized fractional abundance *uaDf5* [(% *uaDf5* day x- % *uaDf5* day
890 1)* % *uaDf5* day 1] in steady-state populations, showing the accumulation rate of mtDNA^{uaDf5} as
891 worms age from day 1 to day 4 of adulthood. **(C)** Analysis of long-lived mutants. **(D)** Analysis of
892 short-lived mutants. **(E)** Analysis of the accumulation of mtDNA^{uaDf5} in PCD mutants. **(F-H)** Linear
893 regression analysis of the normalized fractional abundance mtDNA^{uaDf5} [(% *uaDf5* day x- % *uaDf5*
894 day 1)* % *uaDf5* day 1] in steady-state populations, showing the accumulation rate of mtDNA^{uaDf5}
895 as worms age from day 1 to day 4 of adulthood. **(F)** Analysis of PCD mutants with significantly
896 high steady-state level of mtDNA^{uaDf5}. **(G)** Analysis of PCD mutants with significantly low steady-
897 state level of mtDNA^{uaDf5}. **(H)** Analysis of PCD mutants with no significant change in the steady-
898 state level of mtDNA$^{uaDf5.}$ For **C, D, F, G, and H** dots represent actual datapoints, lines are fitted
899 regression models of the data. For all, n=3 replicates or more of 200 worm populations for each
900 datapoint.
901
902

903 **Supplemental Figure 10**

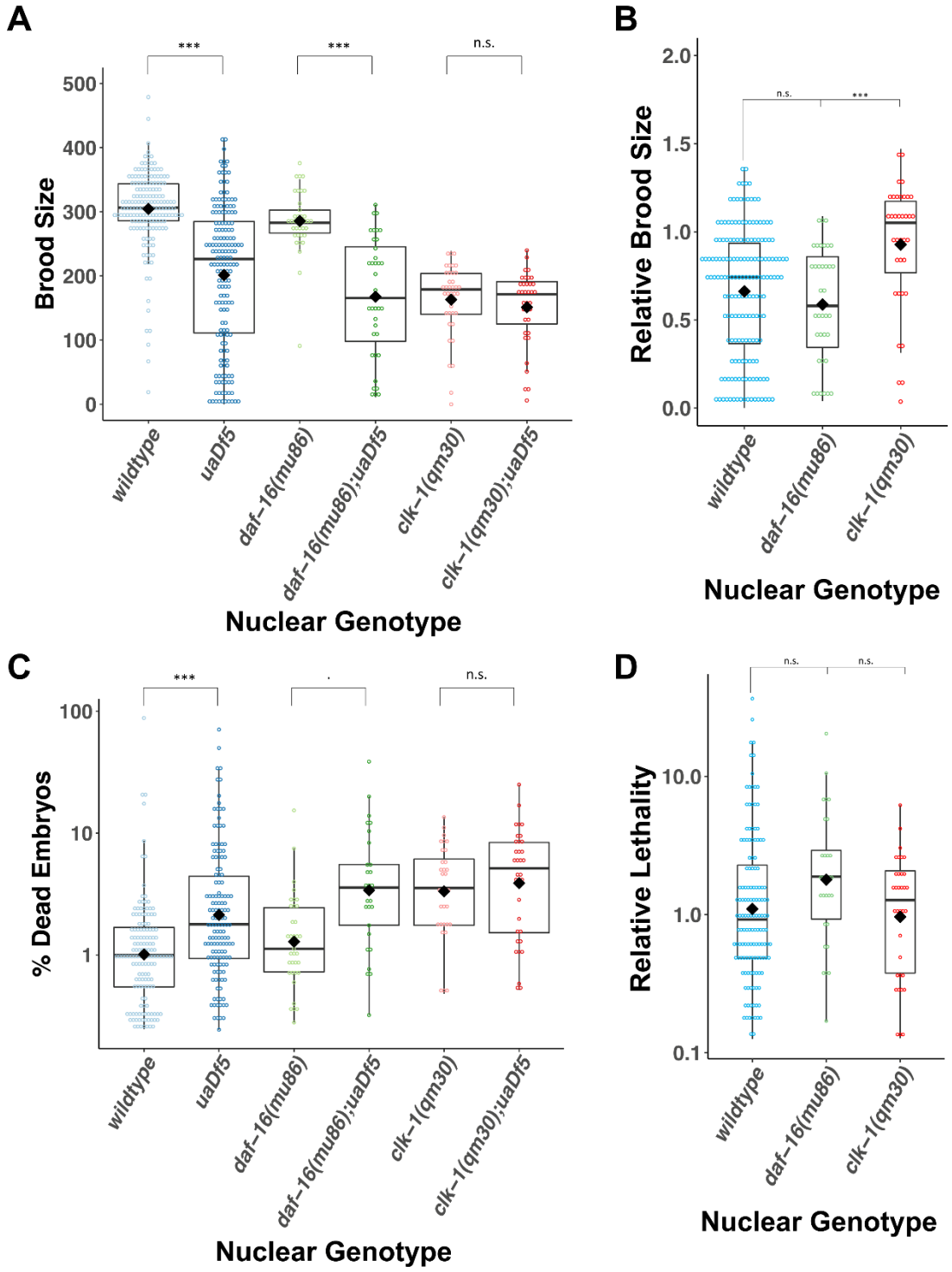

904

905 **Supplemental Figure 10: *uaDf5* differentially impacts fitness parameters in lifespan-affecting**

906 **mutants. (A-B)** Brood size analysis showing how *uaDf5* differentially impacts brood size in

907 lifespan mutant backgrounds. *uaDf5* has no negative impact on the long-lived mutant *clk-1* but
908 has a modestly larger negative impact on the short-lived mutant *daf-16* than it does in the
909 wildtype background. **(B)** Relative brood size of the animals with and without *uaDf5* in the
910 indicated mutant backgrounds. **(C-D)** Embryonic lethality analysis showing how *uaDf5*
911 differentially impacts embryonic lethality in lifespan mutant backgrounds. *uaDf5* has no negative
912 impact on the long-lived mutant *clk-1* but has a modestly larger negative impact on the short-
913 lived mutant *daf-16* than it does in a wildtype background. **(D)** Relative lethality of the animals
914 with and without *uaDf5* in the indicated mutant backgrounds. Box plots show median and IQR,
915 and the diamond indicates the mean. For **A and C**, statistical analysis was performed using the
916 Mann-Whitney test. For **B and D**, statistical analysis was performed using the Kruskal-Wallis test.
917 (*** $p < 0.001$, ** $p < 0.01$, * $p < 0.05$, . $p < 0.1$, n.s. not significant).
918

919 **Supplementary Table 1:** A summary of all mutants analyzed in the PCD pathway, including their
920 known homologs, whether they are part of the core PCD machinery, if they are pro-apoptotic or
921 anti-apoptotic, whether they are mitochondrial proteins, and molecular details of the alleles
922 analyzed.

Gene	Homolog	Core Machinery	Role in Apoptosis	Mitochondrial?	Allele	Parental Strain	Molecular Nature of the Allele	Protein Change
ced-1	SCARF2	N	Pro(engulfment)	N	*e1735*	CB3203	Substitution	Nonsense Q→Ochre
ced-2	CRK	N	Pro(engulfment)	N	*e1752*	CB3257	Substitution	Nonsense W→Opal
ced-3	CASPASE	Y	Pro(executor caspase)	N	*n717*	MT1522	Substitution	Splice site C→T
					n1286	MT3002	Substitution	Nonsense W→Opal
					n718	MT1743	Substitution	Missense G→R
					n2454	MT8354	Substitution	Missense A→T
ced-4	APAF1	Y	Pro(apoptosome)	Y/N (primarily nuclear membrane)	*n1162*	MT2547	Substitution	Nonsense Q→Ochre
					n1894	MT5287	Not curated	Unknown
ced-9	BCL2	Y	Anti	Y	*n1950*	MT4770	Substitution	Missense G→E
ced-10	RAC	N	Pro(engulfment)	N	*n1993*	MT5013	Substitution	Missense V→G
					n3246	MT9958	Substitution	Missense G→R
ced-13	BH3	N	Pro	N	*tm536*	FX536	523bp deletion	Only first 17bp remain
					sv32	MD792	1304bp deletion	Complete knockout, also *inx-5*
csp-1	CASPASE	N	Pro(caspase)	N	*tm917*	JR3196	751bp deletion	Only first 59bp remain
csp-2	CASPASE	N	Anti	N	*tm3077*	JR3397	319bp deletion	Start at position 7317, deletes parts of exon 13

								and all of 14

925 **Supplementary Table 2:** A summary of all lifespan mutants analyzed, including their known

926 homologs, cellular pathways they are known to act in, whether the mutant extends or reduces

927 lifespan, and molecular details of the alleles analyzed.

Gene	Homologs	Pathway	Allele	Parental Strain	Molecular Nature of the Allele	Protein Change	Mutant lifespan	Note
aak-2	AMPK	IIS pathway, adult lifespan, peptidyl-serine phosphorylation, regulation of protein localization	*gt33*	TG38	606bp deletion	Starts at position 3979, deletes exon 3	Decrease	-
			ok524	RB754	408bp deletion	Starts at position 4136, deletes part of exon 3	Decrease	-
clk-1	COQ7	Adult behavior, regulation of cellular metabolism	*qm30*	MQ130	590bp deletion	Starts at position 1044, deletes part of exon 4 and 5	Increase	-
daf-2	IGFR	IIS pathway, cellular response to salt, negative regulator of macromolecule metabolic processes, positive regulation of developmental growth	*e1391*	DR1574	Substitution	Missense P→L	Increase	ts
			e1370	CB1370	Substitution	Missense P→S	Increase	ts
			m41	DR1564	Substitution	Missense G→E	Increase	ts
daf-16	FOXO	IIS pathway, defense response to bacterium, regulation of cellular biosynthetic process, regulation of post-	*mu86*	CF1038	1098bp deletion	Deletes 5 exons	Decrease	-
			mgDf50	GR1307	20193bp deletion with TCTTCATTTTCAG insertion	Deletes 7 exons	Decrease	-

		embryonic development						
fem-3	novel	Male somatic sex determination, masculinization of hermaphrodite germline, positive regulation of macromolecule metabolic process	*q20*	JK816	Not curated	Unknown	Increase	Gof and ts; female germline development inhibited
glp-4	VARS	Cell fate specification, embryonic pattern specification, positive regulation of cell proliferation	*bn2*	SS104	Substitution	Missense G→D	Increase	ts; germline development inhibited

928
929

930 **Supplementary Table 3:** *C. elegans* strains used in this study.

Strain	Genotype	Source
N2	wildtype	CGC
LB138	*him-8(e1489) IV; uaDf5/+*	CGC
JR3630	*N2; uaDf5/+ (8x backcross version of LB138, him(e1489) was outcrossed)*	This study
JR3880	*ced-3(n717) IV; uaDf5/+*	This study
JR4330	*csp-1(tm917) II; uaDf5/+*	This study
JR3977	*ced-3(n1286) IV; uaDf5/+*	This study
JR3955	*ced-13(sv32) X; uaDf5/+*	This study
JR3976	*ced-13(tm536) X; uaDf5/+*	This study
JR3926	*ced-10(n1993) IV; uaDf5/+*	This study
JR4001	*ced-10(n3246) IV; uaDf5/+*	This study
JR3972	*ced-1(e1735) I; uaDf5/+*	This study
JR3978	*ced-2(e1752) IV; uaDf5/+*	This study
JR4010	*ced-1(e1735)I; ced-2(e1752)IV; uaDf5/+*	This study
JR3938	*ced-3(n2454) IV; uaDf5/+*	This study
JR3925	*ced-4(n1162) III; uaDf5/+*	This study
JR4017	*ced-4(n1894) III; uaDf5/+*	This study
JR3986	*csp-2(tm3077) IV; uaDf5/+*	This study
JR4027	*ced-9(n1950) III; uaDf5/+*	This study
JR3983	*ced-3(n718) IV; uaDf5/+*	This study
MT1522	*ced-3(n717) IV*	CGC
FX536	*ced-13(tm536) X*	CGC
JR3966	*glp-4(bn2) I; uaDf5/+*	This study
JR3949	*fem-3(q20) IV; uaDf5/+*	This study
JR3937	*atfs-1(et15) V; uaDf5/+*	This study
JR3960	*daf-2(e1370) III; uaDf5/+*	This study
JR3963	*daf-2(e1391) III; uaDf5/+*	This study
JR3993	*clk-1(qm30) III; uaDf5/+*	This study
JR4060	*daf-2(e1391) clk-1(qm30) III; uaDf5/+*	This study
JR3995	*daf-16(mu86) I; uaDf5/+*	This study
JR3997	*daf-16(mgDf50) I; uaDf5/+*	This study
JR4011	*aak-2(ok524) X; uaDf5/+*	This study
JR4012	*aak-2(gt33) X; uaDf5/+*	This study
JR4008	*daf-16(mu86) I; daf-2(e1391) III; uaDf5/+*	This study
JR4005	*daf-16(mu86) I; daf-2(e1370) III; uaDf5/+*	This study
JR3941	*glp-1(q231) III; uaDf5/+*	This study
CF1038	*daf-16(mu86) I*	CGC
MQ130	*clk-1(qm30) III*	CGC
JR3981	*csp-1(tm917) II; ced-3(n717) IV; uaDf5/+*	This study

931

932

933 **Acknowledgments**

934 We would like to thank the members of the Rothman lab for their support. We thank Jen Smith
935 and the BNL at UCSB for providing excellent facilities which were necessary for this work. We
936 thank Kyle Ploense for his help in statistical analysis. Worm strains used in this work were
937 provided by the Mitani lab, as well as the Caenorhabditis Genetics Center (CGC), which is funded
938 by NIH Office of Research Infrastructure Programs Grant P40 OD010440.

939 **Competing Interests**

940 The authors declare no competing or financial interests.

941 **Author contributions**

942 Sagen E. Flowers - conceptualization, investigation, funding acquisition, writing – original draft
943 preparation, writing – review and editing
944 Rushali Kothari – investigation, writing – review and editing
945 Yamila N. Torres Cleuren - investigation, writing – review and editing
946 Melissa R. Alcorn – statistics, writing – review and editing
947 Chee Kiang Ewe - writing – review and editing
948 Geneva Alok - writing – review and editing
949 Pradeep M. Joshi – conceptualization, investigation, writing – review and editing
950 Joel H. Rothman - conceptualization, supervision, funding acquisition, writing – review and
951 editing

952 **Funding**

953 This work was supported by the grants from the National Institutes of Health (#R01HD082347,
954 #R01HD081266, #R01GM143771, and #R21AG068915).

955 **Data Availability**

956 All data generated or analyzed during this study are included in this article and accompanied
957 supplementary materials.

958 **References**

959 1. YS N, DM T. Mitochondrial disease: genetics and management. J Neurol. J Neurol;
960 2016;263: 179–191. doi:10.1007/S00415-015-7884-3

961 2. PF C. Mitochondrial disease in adults: what's old and what's new? EMBO Mol Med.
962 EMBO Mol Med; 2015;7: 1503–1512. doi:10.15252/EMMM.201505079

963 3. Gorman GS, Schaefer AM, Ng Y, Gomez N, Blakely EL, Alston CL, et al. Prevalence of
964 nuclear and mitochondrial DNA mutations related to adult mitochondrial disease. Ann
965 Neurol. John Wiley & Sons, Ltd; 2015;77: 753–759. doi:10.1002/ANA.24362

966 4. Ghaoui R, Sue CM. Movement disorders in mitochondrial disease. J Neurol. Dr. Dietrich
967 Steinkopff Verlag GmbH and Co. KG; 2018;265: 1230–1240. doi:10.1007/s00415-017-
968 8722-6

969 5. Area-Gomez E, Schon EA. Mitochondrial genetics and disease. Journal of Child Neurology.
970 SAGE Publications Inc.; 2014. pp. 1208–1215. doi:10.1177/0883073814539561

971 6. Dhillon VS, Fenech M. Mutations that affect mitochondrial functions and their
972 association with neurodegenerative diseases. Mutation Research - Reviews in Mutation
973 Research. 2014. pp. 1–13. doi:10.1016/j.mrrev.2013.09.001

974 7. Park CB, Larsson NG. Mitochondrial DNA mutations in disease and aging. Journal of Cell
975 Biology. 2011. pp. 809–818. doi:10.1083/jcb.201010024

976 8. Burté F, Carelli V, Chinnery PF, Yu-Wai-Man P. Disturbed mitochondrial dynamics and

977 neurodegenerative disorders. Nature Reviews Neurology. Nature Publishing Group;
978 2015. pp. 11–24. doi:10.1038/nrneurol.2014.228
979 9. Schon EA, Dimauro S, Hirano M. Human mitochondrial DNA: Roles of inherited and
980 somatic mutations. Nature Reviews Genetics. 2012. pp. 878–890. doi:10.1038/nrg3275
981 10. Brown WM, George M, Wilson AC. Rapid evolution of animal mitochondrial DNA. Proc
982 Natl Acad Sci U S A. 1979;76: 1967–1971. doi:10.1073/pnas.76.4.1967
983 11. Konrad A, Thompson O, Waterston RH, Moerman DG, Keightley PD, Bergthorsson U, et
984 al. Mitochondrial mutation rate, spectrum and heteroplasmy in Caenorhabditis elegans
985 spontaneous mutation accumulation lines of differing population size. Mol Biol Evol.
986 Oxford University Press; 2017;34: 1319–1334. doi:10.1093/molbev/msx051
987 12. Denver DR, Morris K, Lynch M, Vassilieva LL, Thomas WK. High direct estimate of the
988 mutation rate in the mitochondrial genome of Caenorhabditis elegans. Science (80-).
989 2000;289: 2342–2344. doi:10.1126/science.289.5488.2342
990 13. Palozzi JM, Jeedigunta SP, Hurd TR. Mitochondrial DNA Purifying Selection in Mammals
991 and Invertebrates. Journal of Molecular Biology. Academic Press; 2018. pp. 4834–4848.
992 doi:10.1016/j.jmb.2018.10.019
993 14. Stewart JB, Freyer C, Elson JL, Larsson NG. Purifying selection of mtDNA and its
994 implications for understanding evolution and mitochondrial disease. Nature Reviews
995 Genetics. 2008. pp. 657–662. doi:10.1038/nrg2396
996 15. Twig G, Shirihai OS. The interplay between mitochondrial dynamics and mitophagy.
997 Antioxidants and Redox Signaling. 2011. pp. 1939–1951. doi:10.1089/ars.2010.3779
998 16. Busch KB, Kowald A, Spelbrink JN. Quality matters: How does mitochondrial network

999 dynamics and quality control impact on mtDNA integrity? Philosophical Transactions of
1000 the Royal Society B: Biological Sciences. Royal Society of London; 2014.
1001 doi:10.1098/rstb.2013.0442
1002 17. Ni HM, Williams JA, Ding WX. Mitochondrial dynamics and mitochondrial quality control.
1003 Redox Biology. Elsevier B.V.; 2015. pp. 6–13. doi:10.1016/j.redox.2014.11.006
1004 18. Ashrafi G, Schwarz TL. The pathways of mitophagy for quality control and clearance of
1005 mitochondria. Cell Death and Differentiation. 2013. pp. 31–42. doi:10.1038/cdd.2012.81
1006 19. Youle RJ, Narendra DP. Mechanisms of mitophagy. Nat Rev Mol Cell Biol. 2011;12: 9–14.
1007 doi:10.1038/nrm3028
1008 20. Tilokani L, Nagashima S, Paupe V, Prudent J. Mitochondrial dynamics: Overview of
1009 molecular mechanisms. Essays in Biochemistry. Portland Press Ltd; 2018. pp. 341–360.
1010 doi:10.1042/EBC20170104
1011 21. Hernando-Rodríguez B, Artal-Sanz M. Mitochondrial Quality Control Mechanisms and the
1012 PHB (Prohibitin) Complex. Cells. MDPI AG; 2018;7: 238. doi:10.3390/cells7120238
1013 22. Sté phane Rolland AG, Schneid S, Schwarz M, Mokranjac D, Lambie E, Conradt B.
1014 Compromised Mitochondrial Protein Import Acts as a Signal for UPR mt. Cell Rep.
1015 2019;28: 1659–1669. doi:10.1016/j.celrep.2019.07.049
1016 23. Münch C. The different axes of the mammalian mitochondrial unfolded protein response.
1017 BMC Biology. BioMed Central Ltd.; 2018. doi:10.1186/s12915-018-0548-x
1018 24. Callegari S, Dennerlein S. Sensing the stress: A role for the UPR mt and UPR am in the
1019 quality control of mitochondria. Frontiers in Cell and Developmental Biology. Frontiers
1020 Media S.A.; 2018. doi:10.3389/fcell.2018.00031

1021 25. Gitschlag BL, Kirby CS, Samuels DC, Gangula RD, Mallal SA, Patel MR. Homeostatic
1022 Responses Regulate Selfish Mitochondrial Genome Dynamics in C. elegans. Cell Metab.
1023 Cell Press; 2016;24: 91–103. doi:10.1016/j.cmet.2016.06.008
1024 26. Nargund AM, Pellegrino MW, Fiorese CJ, Baker BM, Haynes CM. Mitochondrial import
1025 efficiency of ATFS-1 regulates mitochondrial UPR activation. Science (80-). American
1026 Association for the Advancement of Science; 2012;337: 587–590.
1027 doi:10.1126/science.1223560
1028 27. Lin YF, Schulz AM, Pellegrino MW, Lu Y, Shaham S, Haynes CM. Maintenance and
1029 propagation of a deleterious mitochondrial genome by the mitochondrial unfolded
1030 protein response. Nature. Nature Publishing Group; 2016;533: 416–419.
1031 doi:10.1038/nature17989
1032 28. Murphy CT, Hu PJ. Insulin/insulin-like growth factor signaling in C. elegans [Internet].
1033 WormBook : the online review of C. elegans biology. 2013. pp. 1–43.
1034 doi:10.1895/wormbook.1.164.1
1035 29. Haroon S, Li A, Weinert JL, Fritsch C, Ericson NG, Alexander-Floyd J, et al. Multiple
1036 Molecular Mechanisms Rescue mtDNA Disease in C. elegans. Cell Rep. Elsevier B.V.;
1037 2018;22: 3115–3125. doi:10.1016/j.celrep.2018.02.099
1038 30. Lord CEN, Gunawardena AHLAN. Programmed cell death in C. elegans, mammals and
1039 plants. European Journal of Cell Biology. 2012. pp. 603–613.
1040 doi:10.1016/j.ejcb.2012.02.002
1041 31. Jeong SY, Seol DW. The role of mitochondria in apoptosis. Journal of Biochemistry and
1042 Molecular Biology. 2008. pp. 11–22. doi:10.5483/bmbrep.2008.41.1.011

1043 32. Estaquier J, Vallette F, Vayssiere JL, Mignotte B. The mitochondrial pathways of
1044 apoptosis. Adv Exp Med Biol. 2012;942: 157–183. doi:10.1007/978-94-007-2869-1_7
1045 33. Bhola PD, Letai A. Mitochondria-Judges and Executioners of Cell Death Sentences.
1046 Molecular Cell. Cell Press; 2016. pp. 695–704. doi:10.1016/j.molcel.2016.02.019
1047 34. Tower J. Programmed cell death in aging. Ageing Research Reviews. Elsevier Ireland Ltd;
1048 2015. pp. 90–100. doi:10.1016/j.arr.2015.04.002
1049 35. Larsson N-G. Somatic Mitochondrial DNA Mutations in Mammalian Aging. Annu Rev
1050 Biochem. Annual Reviews; 2010;79: 683–706. doi:10.1146/annurev-biochem-060408-
1051 093701
1052 36. Payne BAI, Chinnery PF. Mitochondrial dysfunction in aging: Much progress but many
1053 unresolved questions. Biochim Biophys Acta. 2015;1847: 1347–53.
1054 doi:10.1016/j.bbabio.2015.05.022
1055 37. Kauppila TES, Kauppila JHK, Larsson NG. Mammalian Mitochondria and Aging: An
1056 Update. Cell Metabolism. Cell Press; 2017. pp. 57–71. doi:10.1016/j.cmet.2016.09.017
1057 38. Conradt B, Wu YC, Xue D. Programmed cell death during Caenorhabditis elegans
1058 development. Genetics. Genetics; 2016;203: 1533–1562.
1059 doi:10.1534/genetics.115.186247
1060 39. Gumienny TL, Lambie E, Hartwieg E, Horvitz HR, Hengartner MO. Genetic control of
1061 programmed cell death in the Caenorhabditis elegans hermaphrodite germline.
1062 Development. 1999;126: 1011–1022. doi:10.5167/uzh-1041
1063 40. Baum JS, St. George JP, McCall K. Programmed cell death in the germline. Seminars in
1064 Cell and Developmental Biology. Elsevier Ltd; 2005. pp. 245–259.

1065 doi:10.1016/j.semcdb.2004.12.008

1066 41. Jaramillo-Lambert A, Ellefson M, Villeneuve AM, Engebrecht JA. Differential timing of S
1067 phases, X chromosome replication, and meiotic prophase in the C. elegans germ line. Dev
1068 Biol. Academic Press Inc.; 2007;308: 206–221. doi:10.1016/j.ydbio.2007.05.019

1069 42. Hafner A, Bulyk ML, Jambhekar A, Lahav G. The multiple mechanisms that regulate p53
1070 activity and cell fate. Nature Reviews Molecular Cell Biology. Nature Publishing Group;
1071 2019. pp. 199–210. doi:10.1038/s41580-019-0110-x

1072 43. Derry WB, Putzke AP, Rothman JH. Caenorhabditis elegans p53: Role in apoptosis,
1073 meiosis, and stress resistance. Science (80-). 2001;294: 591–595.
1074 doi:10.1126/science.1065486

1075 44. Huang W, Jiang T, Choi W, Qi S, Pang Y, Hu Q, et al. Mechanistic insights into CED-4-
1076 mediated activation of CED-3. Genes Dev. Genes Dev; 2013;27: 2039–2048.
1077 doi:10.1101/GAD.224428.113

1078 45. Seshagiri S, Miller LK. Caenorhabditis elegans CED-4 stimulates CED-3 processing and
1079 CED-3-induced. Curr Biol. Cell Press; 1997;7: 455–460. doi:10.1016/S0960-
1080 9822(06)00216-8

1081 46. Tsang WY, Lemire BD. Stable heteroplasmy but differential inheritance of a large
1082 mitochondrial DNA deletion in nematodes. Biochem Cell Biol. 2002;80: 645–654.
1083 doi:10.1139/o02-135

1084 47. Lemire B. Mitochondrial genetics. WormBook. 2005; doi:10.1895/wormbook.1.25.1

1085 48. Van Der Bliek AM, Sedensky MM, Morgan PG. Cell biology of the mitochondrion.
1086 Genetics. Genetics Society of America; 2017;207: 843–871.

1087 doi:10.1534/genetics.117.300262

1088 49. Sousa JS, D'Imprima E, Vonck J. Mitochondrial respiratory chain complexes. Subcellular
1089 Biochemistry. Springer New York; 2018. pp. 167–227. doi:10.1007/978-981-10-7757-9_7

1090 50. Baradaran R, Berrisford JM, Minhas GS, Sazanov LA. Crystal structure of the entire
1091 respiratory complex i. Nature. Nature; 2013;494: 443–448. doi:10.1038/nature11871

1092 51. Song Z, Laleve A, Vallières C, McGeehan JE, Lloyd RE, Meunier B. Human Mitochondrial
1093 Cytochrome b Variants Studied in Yeast: Not All Are Silent Polymorphisms. Hum Mutat.
1094 John Wiley and Sons Inc.; 2016;37: 933–941. doi:10.1002/humu.23024

1095 52. Gartner A, Boag PR, Blackwell TK. Germline survival and apoptosis. WormBook : the
1096 online review of C. elegans biology. 2008. pp. 1–20. doi:10.1895/wormbook.1.145.1

1097 53. Cohen GM. Caspases: The executioners of apoptosis. Biochemical Journal. Portland Press
1098 Ltd; 1997. pp. 1–16. doi:10.1042/bj3260001

1099 54. Shaham S, Reddien PW, Davies B, Horvitz HR. Mutational Analysis of the Caenorhabditis
1100 elegans Cell-Death Gene ced-3. Genetics. 1999;153.

1101 55. Jeong PY, Kumar A, Joshi PM, Rothman JH. Intertwined Functions of Separase and
1102 Caspase in Cell Division and Programmed Cell Death. Sci Rep. Nature Research; 2020;10.
1103 doi:10.1038/s41598-020-63081-w

1104 56. Denning DP, Hatch V, Horvitz HR. Both the Caspase CSP-1 and a Caspase-Independent
1105 Pathway Promote Programmed Cell Death in Parallel to the Canonical Pathway for
1106 Apoptosis in Caenorhabditis elegans. PLoS Genet. 2013;9.
1107 doi:10.1371/journal.pgen.1003341

1108 57. Shaham S. Identification of multiple Caenorhabditis elegans caspases and their potential

1109 roles in proteolytic cascades. J Biol Chem. 1998;273: 35109–35117.
1110 doi:10.1074/jbc.273.52.35109
1111 58. King SD, Gray CF, Song L, Nechushtai R, Gumienny TL, Mittler R, et al. The cisd gene
1112 family regulates physiological germline apoptosis through ced-13 and the canonical cell
1113 death pathway in Caenorhabditis elegans. Cell Death Differ. Nature Publishing Group;
1114 2019;26: 162–178. doi:10.1038/s41418-018-0108-5
1115 59. Schumacher B, Schertel C, Wittenburg N, Tuck S, Mitani S, Gartner A, et al. C. elegans
1116 ced-13 can promote apoptosis and is induced in response to DNA damage. Cell Death
1117 Differ. Nature Publishing Group; 2005;12: 153–161. doi:10.1038/sj.cdd.4401539
1118 60. Fairlie WD, Perugini MA, Kvansakul M, Chen L, Huang DCS, Colman PM. CED-4 forms a 2 :
1119 2 heterotetrameric complex with CED-9 until specifically displaced by EGL-1 or CED-13.
1120 Cell Death Differ. 2006;13: 426–434. doi:10.1038/sj.cdd.4401762
1121 61. Conradt B, Xue D. Programmed cell death. WormBook : the online review of C. elegans
1122 biology. 2005. pp. 1–13. doi:10.1895/wormbook.1.32.1
1123 62. Wu D, Chai Y, Zhu Z, Li W, Ou G, Li W. CED-10-WASP-Arp2/3 signaling axis regulates
1124 apoptotic cell corpse engulfment in C. elegans. Dev Biol. Academic Press Inc.; 2017;428:
1125 215–223. doi:10.1016/j.ydbio.2017.06.005
1126 63. Kinchen JM, Cabello J, Kilngele D, Wong K, Felchtinger R, Schnabel H, et al. Two pathways
1127 converge at CED-10 to mediate actin rearrangement and corpse removal in C. elegans.
1128 Nature. 2005;434: 93–99. doi:10.1038/nature03263
1129 64. Hochreiter-Hufford A, Ravichandran KS. Clearing the dead: Apoptotic cell sensing,
1130 recognition, engulfment, and digestion. Cold Spring Harb Perspect Biol. 2013;5.

1131 doi:10.1101/cshperspect.a008748

1132 65. Wang X, Yang C. Programmed cell death and clearance of cell corpses in Caenorhabditis
1133 elegans. Cellular and Molecular Life Sciences. Birkhauser Verlag AG; 2016. pp. 2221–
1134 2236. doi:10.1007/s00018-016-2196-z

1135 66. Reddien PW, Horvitz HR. THE ENGULFMENT PROCESS OF PROGRAMMED CELL DEATH IN
1136 *CAENORHABDITIS ELEGANS*. Annu Rev Cell Dev Biol. Annual Reviews; 2004;20: 193–221.
1137 doi:10.1146/annurev.cellbio.20.022003.114619

1138 67. Hoeppner DJ, Hengartner MO, Schnabel R. Engulfment genes cooperate with ced-3 to
1139 promote cell death in Caenorhabditis elegans. Nature. Nature Publishing Group;
1140 2001;412: 202–206. doi:10.1038/35084103

1141 68. Geng X, Zhou QH, Kage-Nakadai E, Shi Y, Yan N, Mitani S, et al. Caenorhabditis elegans
1142 caspase homolog CSP-2 inhibits CED-3 autoactivation and apoptosis in germ cells. Cell
1143 Death Differ. 2009;16: 1385–1394. doi:10.1038/cdd.2009.88

1144 69. Yang X, Chang HY, Baltimore D. Essential role of CED-4 oligomerization in CED-3
1145 activation and apoptosis. Science (80-). American Association for the Advancement of
1146 Science; 1998;281: 1355–1357. doi:10.1126/science.281.5381.1355

1147 70. Parsons MJ, Green DR. Mitochondria in cell death. Essays Biochem. 2010;47: 99–114.
1148 doi:10.1042/BSE0470099

1149 71. Harman D. Free radical theory of aging. Mutat Res. 1992;275: 257–266.
1150 doi:10.1016/0921-8734(92)90030-S

1151 72. HARMAN D. Aging: a theory based on free radical and radiation chemistry. J Gerontol.
1152 1956;11: 298–300. doi:10.1093/geronj/11.3.298

1153 73. Szczepanowska K, Trifunovic A. Origins of mtDNA mutations in ageing. Essays in
1154 Biochemistry. Portland Press Ltd; 2017. pp. 325–337. doi:10.1042/EBC20160090
1155 74. Bratic A, Larsson N-G. The role of mitochondria in aging. J Clin Invest. 2013;123: 951–957.
1156 doi:10.1172/JCI64125
1157 75. Ziegler D V., Wiley CD, Velarde MC. Mitochondrial effectors of cellular senescence:
1158 Beyond the free radical theory of aging. Aging Cell. Blackwell Publishing Ltd; 2015. pp. 1–
1159 7. doi:10.1111/acel.12287
1160 76. Kimble J, Crittenden SL. Germline proliferation and its control. WormBook : the online
1161 review of C. elegans biology. 2005. pp. 1–14. doi:10.1895/wormbook.1.13.1
1162 77. Yoon DS, Alfhili MA, Friend K, Lee MH. MPK-1/ERK regulatory network controls the
1163 number of sperm by regulating timing of sperm-oocyte switch in C. elegans germline.
1164 Biochem Biophys Res Commun. Elsevier B.V.; 2017;491: 1077–1082.
1165 doi:10.1016/j.bbrc.2017.08.014
1166 78. Angeles-Albores D, Leighton DHW, Tsou T, Khaw TH, Antoshechkin I, Sternberg PW. The
1167 Caenorhabditis elegans female-like state: Decoupling the transcriptomic effects of aging
1168 and sperm status. G3 Genes, Genomes, Genet. Genetics Society of America; 2017;7:
1169 2969–2977. doi:10.1534/g3.117.300080
1170 79. Kujoth CC, Hiona A, Pugh TD, Someya S, Panzer K, Wohlgemuth SE, et al. Medicine:
1171 Mitochondrial DNA mutations, oxidative stress, and apoptosis in mammalian aging.
1172 Science (80-). American Association for the Advancement of Science; 2005;309: 481–
1173 484. doi:10.1126/science.1112125
1174 80. Beanan MJ, Strome S. Characterization of a germ-line proliferation mutation in C.

1175 elegans. Development. 1992;116.

1176 81. Barton MK, Schedl TB, Kimble J. Gain-of-function mutations of fem-3, a sex-
1177 determination gene in Caenorhabditis elegans. Genetics. 1987;115: 107–119.

1178 82. Bartke A. Insulin and aging. Cell Cycle. Taylor and Francis Inc.; 2008. pp. 3338–3343.
1179 doi:10.4161/cc.7.21.7012

1180 83. Anisimov VN, Bartke A. The key role of growth hormone-insulin-IGF-1 signaling in aging
1181 and cancer. Critical Reviews in Oncology/Hematology. 2013. pp. 201–223.
1182 doi:10.1016/j.critrevonc.2013.01.005

1183 84. Piper MDW, Selman C, McElwee JJ, Partridge L. Separating cause from effect: how does
1184 insulin/IGF signalling control lifespan in worms, flies and mice? J Intern Med. John Wiley
1185 & Sons, Ltd; 2008;263: 179–191. doi:10.1111/J.1365-2796.2007.01906.X

1186 85. Kenyon C, Chang J, Gensch E, Rudner A, Tabtiang R. A C. elegans mutant that lives twice
1187 as long as wild type. Nature. 1993;366: 461–464. doi:10.1038/366461a0

1188 86. Tatar M, Kopelman A, Epstein D, Tu M-P, Yin C-M, Garofalo RS. A Mutant Drosophila
1189 Insulin Receptor Homolog That Extends Life-Span and Impairs Neuroendocrine Function.
1190 Science (80-). American Association for the Advancement of Science; 2001;292: 107–
1191 110. doi:10.1126/SCIENCE.1057987

1192 87. Blüher M, Kahn BB, Kahn CR. Extended Longevity in Mice Lacking the Insulin Receptor in
1193 Adipose Tissue. Science (80-). American Association for the Advancement of Science;
1194 2003;299: 572–574. doi:10.1126/SCIENCE.1078223

1195 88. Gitschlag BL, Tate AT, Patel MR. Nutrient status shapes selfish mitochondrial genome
1196 dynamics across different levels of selection. Elife. eLife Sciences Publications Ltd;

1197 2020;9: 1–27. doi:10.7554/ELIFE.56686

1198 89. Apfeld J, O'Connor G, McDonagh T, DiStefano PS, Curtis R. The AMP-activated protein
1199 kinase AAK-2 links energy levels and insulin-like signals to lifespan in C. elegans. Genes
1200 Dev. Cold Spring Harbor Laboratory Press; 2004;18: 3004–3009.
1201 doi:10.1101/gad.1255404

1202 90. Miyadera H, Kano K, Miyoshi H, Ishii N, Hekimi S, Kita K. Quinones in long-lived clk-1
1203 mutants of Caenorhabditis elegans. FEBS Lett. No longer published by Elsevier; 2002;512:
1204 33–37. doi:10.1016/S0014-5793(02)02282-2

1205 91. Miyadera H, Amino H, Hiraishi A, Taka H, Murayama K, Miyoshi H, et al. Altered Quinone
1206 Biosynthesis in the Long-lived clk-1Mutants of Caenorhabditis elegans. J Biol Chem.
1207 Elsevier; 2001;276: 7713–7716. doi:10.1074/JBC.C000889200

1208 92. Kirby CS, Patel MR. Elevated mitochondrial DNA copy number found in ubiquinone-
1209 deficient clk-1 mutants is not rescued by ubiquinone precursor 2-4-dihydroxybenzoate.
1210 Mitochondrion. Elsevier B.V.; 2021;58: 38–48. doi:10.1016/j.mito.2021.02.001

1211 93. Charmpilas N, Tavernarakis N. Mitochondrial maturation drives germline stem cell
1212 differentiation in Caenorhabditis elegans. Cell Death Differ. Springer Nature; 2020;27:
1213 601–617. doi:10.1038/s41418-019-0375-9

1214 94. Folmes CDL, Ma H, Mitalipov S, Terzic A. Mitochondria in pluripotent stem cells:
1215 Stemness regulators and disease targets. Current Opinion in Genetics and Development.
1216 Elsevier Ltd; 2016. pp. 1–7. doi:10.1016/j.gde.2016.02.001

1217 95. Floros VI, Pyle A, DIetmann S, Wei W, Tang WWC, Irie N, et al. Segregation of
1218 mitochondrial DNA heteroplasmy through a developmental genetic bottleneck in human

1219 embryos. Nat Cell Biol. 2018; 144–151. doi:10.1038/s41556-017-0017-8

1220 96. Zhang H, Burr SP, Chinnery PF. The mitochondrial DNA genetic bottleneck: Inheritance
1221 and beyond. Essays in Biochemistry. Portland Press Ltd; 2018. pp. 225–234.
1222 doi:10.1042/EBC20170096

1223 97. Wai T, Teoli D, Shoubridge EA. The mitochondrial DNA genetic bottleneck results from
1224 replication of a subpopulation of genomes. Nat Genet. 2008; 1484–1488.
1225 doi:10.1038/ng.258

1226 98. Liau WS, Gonzalez-Serricchio AS, Deshommes C, Chin K, LaMunyon CW. A persistent
1227 mitochondrial deletion reduces fitness and sperm performance in heteroplasmic
1228 populations of C. elegans. BMC Genet. BioMed Central; 2007;8: 1–11. doi:10.1186/1471-
1229 2156-8-8

1230 99. Zhu Z, Han X, Wang Y, Liu W, Lu Y, Xu C, et al. Identification of Specific Nuclear Genetic
1231 Loci and Genes That Interact With the Mitochondrial Genome and Contribute to
1232 Fecundity in Caenorhabditis elegans. Front Genet. Frontiers; 2019;10: 28.
1233 doi:10.3389/fgene.2019.00028

1234 100. Levin L, Blumberg A, Barshad G, Mishmar D. Mito-nuclear co-evolution: The positive and
1235 negative sides of functional ancient mutations. Front Genet. Frontiers Media S.A.;
1236 2014;5: 448. doi:10.3389/fgene.2014.00448

1237 101. Paliwal S, Fiumera AC, Fiumera HL. Mitochondrial-nuclear epistasis contributes to
1238 phenotypic variation and coadaptation in natural isolates of saccharomyces cerevisiae.
1239 Genetics. Genetics Society of America; 2014;198: 1251–1265.
1240 doi:10.1534/genetics.114.168575

1241 102. Zhu CT, Ingelmo P, Rand DM. G×G×E for Lifespan in Drosophila: Mitochondrial, Nuclear,
1242 and Dietary Interactions that Modify Longevity. PLoS Genet. Public Library of Science;
1243 2014;10. doi:10.1371/journal.pgen.1004354
1244 103. Meiklejohn CD, Holmbeck MA, Siddiq MA, Abt DN, Rand DM, Montooth KL. An
1245 Incompatibility between a Mitochondrial tRNA and Its Nuclear-Encoded tRNA Synthetase
1246 Compromises Development and Fitness in Drosophila. PLoS Genet. Public Library of
1247 Science; 2013;9. doi:10.1371/journal.pgen.1003238
1248 104. Dingley SD, Polyak E, Ostrovsky J, Srinivasan S, Lee I, Rosenfeld AB, et al. Mitochondrial
1249 DNA Variant in COX1 Subunit Significantly Alters Energy Metabolism of Geographically
1250 Divergent Wild Isolates in Caenorhabditis elegans. J Mol Biol. 2014;426: 2199–2216.
1251 doi:10.1016/j.jmb.2014.02.009
1252 105. Yee C, Yang W, Hekimi S. The intrinsic apoptosis pathway mediates the pro-longevity
1253 response to mitochondrial ROS in C. elegans. Cell. PMC Canada manuscript submission;
1254 2014;157: 897. doi:10.1016/J.CELL.2014.02.055
1255 106. H H, C K. Signals from the reproductive system regulate the lifespan of C. elegans.
1256 Nature. Nature; 1999;399: 362–366. doi:10.1038/20694
1257 107. L D, CW A, S K. New insights into apoptosome structure and function. Cell Death Differ.
1258 Cell Death Differ; 2018;25: 1194–1208. doi:10.1038/S41418-017-0025-Z
1259 108. S Y, X Y, JM A, JE H, SJ L, CW A. The holo-apoptosome: activation of procaspase-9 and
1260 interactions with caspase-3. Structure. Structure; 2011;19: 1084–1096.
1261 doi:10.1016/J.STR.2011.07.001
1262 109. Zermati Y, Mouhamad S, Stergiou L, Besse B, Galluzzi L, Boehrer S, et al. Nonapoptotic

1263 Role for Apaf-1 in the DNA Damage Checkpoint. Mol Cell. Cell Press; 2007;28: 624–637.
1264 doi:10.1016/j.molcel.2007.09.030
1265 110. Ferraro E, Pesaresi MG, De Zio D, Cencioni MT, Gortat A, Cozzolino M, et al. Apaf1 plays a
1266 pro-survival role by regulating centrosome morphology and function. J Cell Sci. 2011;124:
1267 3450–3463. doi:10.1242/jcs.086298
1268 111. Liu WH, Lin YL, Wang JP, Liou W, Hou RF, Wu YC, et al. Restriction of vaccinia virus
1269 replication by a ced-3 and ced-4-dependent pathway in Caenorhabditis elegans. Proc
1270 Natl Acad Sci U S A. National Academy of Sciences; 2006;103: 4174–4179.
1271 doi:10.1073/pnas.0506442103
1272 112. Wang G, Sun L, Reina CP, Song I, Gabel C V., Driscoll M. CED-4 CARD domain residues can
1273 modulate non-apoptotic neuronal regeneration functions independently from apoptosis.
1274 Sci Rep. 2019;9: 13315. doi:10.1038/s41598-019-49633-9
1275 113. Chaudhary D, O'Rourke K, Chinnaiyan AM, Dixit VM. The Death Inhibitory Molecules CED-
1276 9 and CED-4L Use a Common Mechanism to Inhibit the CED-3 Death Protease. J Biol
1277 Chem. Elsevier; 1998;273: 17708–17712. doi:10.1074/JBC.273.28.17708
1278 114. Mack HID, Zhang P, Fonslow BR, Yates JR. The protein kinase MBK-1 contributes to
1279 lifespan extension in daf-2 mutant and germline-deficient Caenorhabditis elegans. Aging
1280 (Albany NY). Impact Journals LLC; 2017;9: 1414–1432. doi:10.18632/aging.101244
1281 115. Libina N, Berman JR, Kenyon C. Tissue-Specific Activities of C. elegans DAF-16 in the
1282 Regulation of Lifespan. Cell. Cell Press; 2003;115: 489–502. doi:10.1016/S0092-
1283 8674(03)00889-4
1284 116. Lapierre LR, Hansen M. Lessons from C. elegans: signaling pathways for longevity. Trends

1285 Endocrinol Metab. Elsevier Current Trends; 2012;23: 637–644.
1286 doi:10.1016/J.TEM.2012.07.007
1287 117. A A. Regulation of longevity by the reproductive system. Exp Gerontol. Exp Gerontol;
1288 2013;48: 596–602. doi:10.1016/J.EXGER.2012.09.009
1289 118. Branicky R, Bénard C, Hekimi S. clk-1, mitochondria, and physiological rates. BioEssays.
1290 2000. pp. 48–56. doi:10.1002/(SICI)1521-1878(200001)22:1<48::AID-BIES9>3.0.CO;2-F
1291 119. Hekimi S, Guarente L. Genetics and the specificity of the aging process. Science. 2003. pp.
1292 1351–1354. doi:10.1126/science.1082358
1293 120. Blackwell TK, Steinbaugh MJ, Hourihan JM, Ewald CY, Isik M. SKN-1/Nrf, stress responses,
1294 and aging in Caenorhabditis elegans. Free Radic Biol Med. Pergamon; 2015;88: 290–301.
1295 doi:10.1016/J.FREERADBIOMED.2015.06.008
1296 121. Youle RJ, Van Der Bliek AM. Mitochondrial fission, fusion, and stress. Science. American
1297 Association for the Advancement of Science; 2012. pp. 1062–1065.
1298 doi:10.1126/science.1219855
1299 122. Twig G, Elorza A, Molina AJA, Mohamed H, Wikstrom JD, Walzer G, et al. Fission and
1300 selective fusion govern mitochondrial segregation and elimination by autophagy. EMBO
1301 J. 2008;27: 433–446. doi:10.1038/sj.emboj.7601963
1302 123. Stiernagle T. Maintenance of C. elegans. WormBook : the online review of C. elegans
1303 biology. 2006. pp. 1–11. doi:10.1895/wormbook.1.101.1
1304 124. C. elegans Deletion Mutant Consortium. large-scale screening for targeted knockouts in
1305 the Caenorhabditis elegans genome. G3 (Bethesda). 2012;2: 1415–25.
1306 doi:10.1534/g3.112.003830

1307 125. Li H, Durbin R. Fast and accurate short read alignment with Burrows–Wheeler transform.
1308 Bioinformatics. Oxford Academic; 2009;25: 1754–1760.
1309 doi:10.1093/BIOINFORMATICS/BTP324
1310 126. Li H, Handsaker B, Wysoker A, Fennell T, Ruan J, Homer N, et al. The Sequence
1311 Alignment/Map format and SAMtools. Bioinformatics. Oxford Academic; 2009;25: 2078–
1312 2079. doi:10.1093/BIOINFORMATICS/BTP352
1313 127. Koboldt DC, Chen K, Wylie T, Larson DE, McLellan MD, Mardis ER, et al. VarScan: variant
1314 detection in massively parallel sequencing of individual and pooled samples.
1315 Bioinformatics. Oxford Academic; 2009;25: 2283–2285.
1316 doi:10.1093/BIOINFORMATICS/BTP373
1317
1318